



Effect of bone marrow mesenchymal stem cells-derived exosomes on diabetes-induced retinal injury: Implication of Wnt/ b-catenin signaling pathway

Nesrine Ebrahim^{a,b}, Heba Elsayed Abd El-Halim^a, Omayma Kamel Helal^a, Nahla El-Eraky El-Azab^a, Omnia A.M. Badr^c, Amira Hassouna^d, Hajir A.Al Saihati^e, Nashwa Hassan Aborayah^f, Hanan Tawfeek Emam^f, Hend S. El-wakeel^g, Mohammad Aljasir^h, Mohamed El-Sherbiny^{i,j}, Naglaa A.S. Sarg^k, Gehan Ahmed Shaker^l, Ola Mostafa^a, Dina Sabry^{m,n}, Marwa Abdel Kader Fouly^o, Nicholas Robert Forsyth^p, Nehal M. Elsherbiny^{q,r,*}, Rabab F. Salim^{s,**}

^a Department of Histology and Cell Biology, Faculty of Medicine, Benha University, Egypt

^b Stem Cell Unit, Faculty of Medicine, Benha University, Egypt

^c Department of Genetics and Genetic Engineering, Faculty of Agriculture, Benha University, Egypt

^d School of Interprofessional Health Studies, Faculty of Health and Environmental Sciences, AUT University, Auckland, New Zealand

^e Department of Clinical Laboratory Sciences, College of Applied Medical Sciences, University of Hafr Albatin, Saudi Arabia

^f Department of Clinical Pharmacology, Faculty of Medicine, Benha University, Egypt

^g Department of Physiology, Faculty of Medicine, Benha University, Egypt

^h Department of Medical Laboratories, College of Applied Medical Sciences, Qassim University, Buraydah, Saudi Arabia

ⁱ Department of Basic Medical Sciences, College of Medicine, AlMaarefa University, P.O. Box 71666, Riyadh, 11597, Saudi Arabia

^j Department of Anatomy, Mansoura Faculty of Medicine, Mansoura University, Egypt

^k Department of Anatomy, Benha Faculty of Medicine, Benha University, Egypt

^l Department of Medical Physiology, Faculty of Medicine, Mansoura University, Mansoura, Egypt

^m Department of Medical Biochemistry and Molecular Biology, Faculty of Medicine, Cairo University, Egypt

ⁿ Department of Medical Biochemistry and Molecular Biology, Faculty of Medicine, Badr University, Cairo 11562, Egypt

^o Research Institute of Ophthalmology, Cairo, Egypt

^p Guy Hilton Research Laboratories, School of Pharmacy and Bioengineering, Faculty of Medicine and Health Sciences, Keele University, Newcastle ST5 5BG, UK

^q Department of Pharmaceutical Chemistry, Faculty of Pharmacy, University of Tabuk, Tabuk, Saudi Arabia

^r Biochemistry department, Faculty of Pharmacy, Mansoura University, 35516, Mansoura, Egypt

^s Department of Medical Biochemistry and Molecular Biology, Faculty of Medicine, Benha University, Egypt

ARTICLE INFO

Keywords:

Diabetic retinopathy
Mesenchymal stem cells
Exosomes

ABSTRACT

Background: Diabetic retinopathy (DR) is a serious microvascular complication of diabetes mellitus. Mesenchymal stem cells are currently studied as therapeutic strategy for management of DR. Exosomes, considered as a promising cell-free therapy option, display biological functions similar to those of their parent cells. In retinal development, Wnt/b-catenin signaling provides key cues for functional progression. The present study aimed to

Abbreviations: Anti-VEGF, anti-vascular endothelial growth factor; BM-MSCs-Ex, bone marrow-derived mesenchymal stem cell-derived exosomes; DM, diabetes mellitus; DR, diabetic retinopathy; Fz, frizzled; GCL, ganglionic cell layer; GFAP, glial fibrillary acidic protein; GSK3b, glycogen synthase kinase-3b; IHC, immunohistochemistry; ILM, inner limiting membrane; INL, inner nuclear layer; IPL, inner plexiform layer; LRP5/6, low-density lipoprotein receptor-related protein; NFL, nerve fiber layer; OLM, outer limiting membrane; ONL, outer nuclear layer; PRL, photoreceptor layer; RPE, retinal pigment epithelial; STZ, streptozotocin; TNF- α , tumor necrosis factor- α .

* Corresponding author at: Department of Pharmaceutical Chemistry, Faculty of Pharmacy, University of Tabuk, Tabuk, Saudi Arabia.

** Corresponding author.

E-mail addresses: Nesrien.saleem@fmed.bu.edu.eg (N. Ebrahim), omnia.badr@fagr.bu.edu.eg (O.A.M. Badr), Amirahassouna@kasralainy.edu.eg (A. Hassouna), hajirsh@uhb.edu.sa (H.A. Al Saihati), NASHWA.ABORAYAH@fmed.bu.edu.eg (N.H. Aborayah), hanantawfeek@yahoo.com (H.T. Emam), Dr_physiology_dep@yahoo.com (H.S. El-wakeel), mjasr@qu.edu.sa (M. Aljasir), msharbini@mcst.edu.sa (M. El-Sherbiny), nagla.srg@find.bu.edu.eg (N.A.S. Sarg), gehanshaker@mans.edu.eg (G.A. Shaker), ola.mostafa.moez@gmail.com (O. Mostafa), dinasabry@kasralainy.edu.eg (D. Sabry), marwa.rio2014@gmail.com (M.A.K. Fouly), n.r.forsyth@keele.ac.uk (N.R. Forsyth), drnehal@hotmail.com (N.M. Elsherbiny), rabab.bio@yahoo.com (R.F. Salim).

<https://doi.org/10.1016/j.bioph.2022.113554>

Received 24 May 2022; Received in revised form 1 August 2022; Accepted 14 August 2022

Available online 17 August 2022

0753-3322/© 2022 The Author(s). Published by Elsevier Masson SAS. This is an open access article under the CC BY-NC-ND license (<http://creativecommons.org/licenses/by-nc-nd/4.0/>).

Wnt/ b-catenin signaling
Oxidative stress
Angiogenesis

evaluate the potential efficacy of bone marrow-derived mesenchymal stem cell-derived exosomes (BM-MSCs-Ex) in diabetes-induced retinal injury via modulation of the Wnt/ b-catenin signaling pathway.

Methods: Eighty-one rats were allocated into 6 groups (control, DR, DR + DKK1, DR + exosomes, DR + Wnt3a and DR + exosomes+Wnt3a). Evaluation of each group was via histopathological examination, assessment of gene and/or protein expression concerned with oxidative stress (*SOD1*, *SOD2*, *Nox2*, *Nox4*, *iNOS*), inflammation (*TNF- α* , *ICAM-1*, *NF- κ B*) and angiogenesis (*VEGF*, *VE-cadherin*).

Results: Results demonstrated that exosomes blocked the wnt/b-catenin pathway in diabetic retina concomitant with significant reduction of features of DR as shown by downregulation of retinal oxidants, upregulation of antioxidant enzymes, suppression of retinal inflammatory and angiogenic markers. These results were further confirmed by histopathological results, fundus examination and optical coherence tomography. Additionally, exosomes ameliorative effects abrogated wnt3a-triggered retinal injury in DR.

Conclusion: Collectively, these data demonstrated that exosomes ameliorated diabetes-induced retinal injury via suppressing Wnt/ b-catenin signaling with subsequent reduction of oxidative stress, inflammation and angiogenesis.

1. Introduction

Diabetic retinopathy (DR), a common microvascular complication of diabetes mellitus (DM), results in retinal vascular leakage, inflammation, and aberrant neovascularization and is considered a primary cause of blindness in the working-age population [1,2]. The incidence of diabetes increases every year, with an estimated 451 million people suffering from the disease in 2017 and a predicted increased incidence to 693 million people by 2045 [3]. Most patients with type 1 diabetes will ultimately develop DR, with a further 50–80% patients with type 2 diabetes likely to develop DR with 20–25 years of diabetes diagnosis [4].

Laser photocoagulation and anti-vascular endothelial growth factor (anti-VEGF) therapy are currently considered standard-of-care treatments. Laser photocoagulation therapy targets advanced stages of disease [5] and while anti-VEGF medication can reduce vascular permeability and halt the course of DR, trials have shown that it was not successful for all individuals, and that some patient responses to therapy wane over time [6]. New DR therapeutic options are therefore urgently required. Understanding the underlying mechanisms of DR is essential for the development of new therapeutic approaches. Proangiogenic signaling pathways as well as inflammatory cytokines have now been implicated in DR pathogenesis in addition to *VEGF* [7].

The Wnt signaling pathway plays a key role in a variety of physiological and pathological processes, including angiogenesis and inflammation [8–12]. Wnt pathways can be classified into two types, canonical and noncanonical. Binding of Wnt to the co-receptor complex of Frizzled (Fz) and low-density lipoprotein receptor-related protein (LRP5/6) inactivates Glycogen synthase kinase-3b (GSK3b) and induces b-catenin translocation to the nucleus, where it forms a complex with T-cell factor/lymphoid enhancer factor (TCF4/LEF) to stimulate the production of Wnt target genes like *VEGF* [13,14]. The canonical b-catenin-dependent Wnt pathway is important for retinal microvasculature growth and differentiation [15]. Dysregulated canonical Wnt signaling in DR promoted pathogenic processes. On the other hand, Wnt antagonists have been considered as therapies for neovascular disorders due to the importance of Wnt signaling in angiogenesis [12].

Mesenchymal stem cells (MSCs) are multipotent stem cells. In regenerative medicine, they are amongst the most widely used cells for both laboratory research and clinical trial [16]. MSCs are thought to stimulate tissue regeneration either directly, through their differentiation into a variety of mesenchymal cell lineages, or indirectly, via their secretion of bioactive factors alone or packaged in exosomes that can provide cell-to-cell signaling and activate regenerative pathways in host tissues [17].

Exosomes are nanoscale vesicles of endocytic origins that have an ability to play a key role in cell-to-cell communication with potential use in novel therapeutic approaches [18–20]. Exosomes themselves are a discrete population of vesicles with dimensions ranging from 30 to 150 nanometers [21]. These membrane-enclosed vesicles transport a variety of functional proteins, microRNAs, and mRNAs, transferring

information between cells and mediating a variety of physiological and pathological processes [22]. MSC-derived exosomes enhance regeneration of damaged tissue and present a unique therapeutic technique for application across a range of tissue types, including heart, bone, cartilage, retina, liver, neuron, and skin [23,24]. Intriguingly, MSC derived exosomes contain anti-angiogenic miRNAs including miR-16 and miR-100, which inhibit angiogenesis via targeting *VEGF* [25]. Recently, Gu et al. [26] displayed that adipose MSC-derived exosomes suppressed inflammatory response and angiogenesis in DR via miR-192 release. Additionally, Bauchl et al. [27] revealed that exosomes control angiogenic activity through regulation of endothelial cell viability, proliferation, and the tube-like generation. *In vivo*, exosomes reduced the generation of endothelial vessel-like structures, associated with a reduced proportion of endothelial cells. BM-MSCs-Exosomes down-regulated the expression of numerous proteins (b-catenin, Wnt3a and Wnt10b) in the Wnt signaling pathway, contributed subsequently to inhibition of downstream gene expression (*Cyclin D1* and *WISP1*). Further, MSC-derived exosomes transport miR-133b, which inhibited the Wnt/b-catenin signaling pathway via suppression of *EZH2* [28]. Nevertheless, the effect of MSC-exosomes on Wnt/b-catenin signaling in DR has not been fully investigated.

Therefore, current work aims to understand the molecular mechanisms by which the exosomes derived from bone marrow MSCs could alleviate diabetes-induced retinal injury via Wnt/b-catenin signaling regulation. We show that BM-MSCs-Exosomes ameliorate features of retinal injury in experimental model of diabetes. BM-MSCs-exosomes treatment suppressed Wnt/ b-catenin signaling, combated oxidative stress, inflammation and angiogenesis.

2. Materials and methods

2.1. Experimental animals

Eight weeks aged adult male albino rats (weighing 250–270 g) were obtained from the Experimental Animal Unit, Faculty of Veterinary Medicine, Benha University, Egypt. Rats were housed in clean cages and allowed free access to standard rodent diet and clean tap water. Animals were allowed to adapt to lab environment which was controlled in terms of room temperature (23 ± 3 °C) and light (12 h cycle starting at 8:00 AM). All experimental procedures followed the guides of institutional review board for animal experiments (Faculty of Medicine, Benha University, Benha, Egypt). All experiments strictly adhered to National Institutes of Health Guide for the Care and Use of Laboratory Animals (NIH publication 85–23, revised 2011).

2.1.1. Preparation of MSCs-derived exosomes

Supernatant of bone-marrow derived MSCs (BM-MSCs), representing conditioned media was used for preparation of MSCs-derived exosomes. Rat BM-MSCs were prepared in the Central Lab, Faculty of Medicine, Benha University according to previous description [29,30]. BM-MSCs

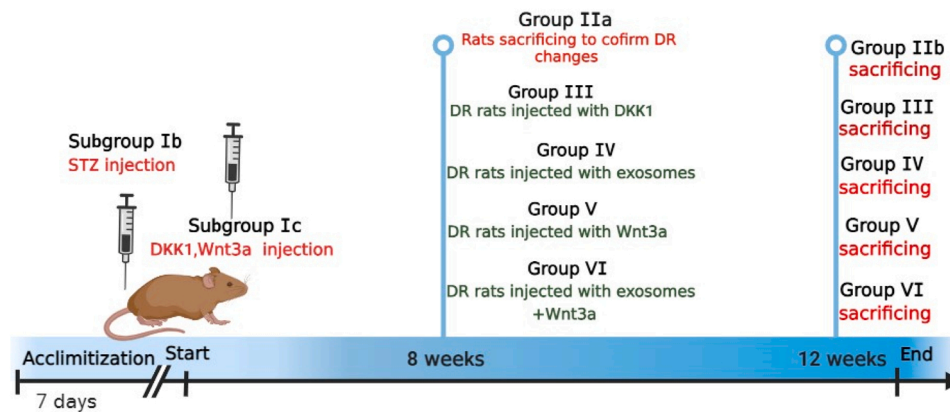


Fig. 1. Timeline for experimental design.

were cultured overnight in fetal bovine serum-free Dulbecco's Modified Eagle Medium (DMEM) containing 0.5% human serum albumin (HSA) (Sigma-Aldrich, St. Louis, MO, USA). Viability of cells cultured overnight was confirmed with Trypan blue exclusion which revealed more than 99% viability. Thereafter, cells were plated for 7 days at 4000 cells/cm². On day 7, cells were trypsinized, counted and re-incubated in expansion medium for another seven days at a density of 2000 cells/cm² (end of the first passage). Cells' expansion was repeated until the third passage. This was followed by conditioned medium collection and storage at -80 °C. To isolate exosomes, medium was centrifuged for 20 min at 2000 g to remove debris followed by ultracentrifugation at 100,000g for 1 h using a SW41 swing rotor at 4 °C (Beckman Coulter, Fullerton, CA, USA). Following isolation, exosomes were washed with solution consisting of serum-free M199 mixed with 25 mM 4-(2-hydroxyethyl)-1-piperazineethanesulfonic acid (HEPES) (pH = 7.4) (Sigma-Aldrich, St. Louis, MO, USA), and then ultracentrifugation in the same conditions. Finally, exosomes were collected, characterized, and then kept at -80 °C for further use.

2.1.2. MSC-derived exosome characterization

Exosomes were isolated from the supernatant of MSCs cultured in FBS free DMEM (the first, second, and third passages). The isolated exosomes were fixed by incubation in 2.5% glutaraldehyde in human serum albumin (HSA) for 2 h. The vesicles were then washed, ultracentrifuged and resuspended in HSA (100 µl). Twenty microliters of exosomes were loaded onto a formvar/carbon-coated grid, negatively stained with 3% aqueous phosphor-tungstic acid for 1 min, and observed by transmission electron microscopy (Hitachi H-7650, Hitachi, Tokyo, Japan) [31]. Bradford method (BioRad, Hercules, CA, USA) was used to quantify the protein content of exosomes. Additionally, PKH-26 (Sigma-Aldrich, St. Louis, MO, USA) was used to confirm exosomal localization within the retinal tissue. Briefly, the exosome pellet was diluted to 1 ml with PKH-26 kit solution. Then, fluorochrome (2 µl) was added to exosomes suspension and incubated for 15 min at 38.5 °C. After that, exosomes suspension was mixed with serum-free HG-DMEM (7 ml) and ultracentrifuged at 100,000g and 4 °C for 1 h. The final pellet was rapidly resuspended in HG-DMEM and then stored at -80 °C until used for injection in experimental animals [32].

2.1.3. Iron oxide for direct labelling of MSCs

MSCs were incubated for 30 min in 4 ml RPMI media containing 50 µm iron oxide [33]. Cells were then centrifuged for 10 min at 2000 rpm to separate iron labelled MSCs. Labeled MSCs released exosomes that contained iron oxide [34].

2.1.4. Prussian blue staining

Retinal sections were treated with acid solutions of ferrocyanides. Ferrocyanide reacts with ferric ion (+3) in the retinal tissues to produce

ferric ferrocyanide, a bright blue pigment called Prussian blue. Iron labeled injected MSCs were detected in retinal tissue sections by Prussian blue staining using eosin as a counter stain [35].

2.1.5. Experimental Chemicals

Streptozotocin (STZ) was purchased from (Sigma Chemical Co., St. Louis, USA) as a white powder. It was freshly prepared in 0.1 M cold citrate buffer (pH 4.5) and was injected intraperitoneal (IP) at a single dose of (60 mg/kg) [30].

Recombinant Mouse Dkk-1 (Catalog Number: 5897-DK-010/CF, R&D Systems, Bio-techno brand); DKK1 100 µg/ml.

Recombinant Mouse Wnt3a (Catalog Number: 1324-WN, R&D Systems, Bio-techno brand); Wnt3a 40 µg/ml.

2.1.6. Induction of diabetes mellitus type I rat model

Type I diabetes mellitus (DM) was induced according to a previously described protocol [30]. Overnight fasted rats were injected IP by a single dose (60 mg/kg) of STZ. To reduce the early death due to discharge of insulin from partially injured pancreas, rats were provided with drinking water containing (15 g/L) sucrose for two days following STZ injection. Then, rats were checked for induction of hyperglycaemia 72 hr later, and measured blood sugar greater than 250 mg/dl was considered diabetic and included in the study. To avoid consequent development of ketonuria, diabetic rats received subcutaneous injection of long-acting insulin (2-4 U/rat) to keep blood glucose levels in a desirable range (about 350 mg/dl).

2.2. Experimental design

After one week of acclimatization, 81 adult rats were randomly divided into six groups:

Group I (control group; n = 27): The rats were divided equally into three subgroups:

Subgroup Ia: The rats were maintained under similar laboratory conditions without intervention.

Subgroup Ib: The rats were injected with vehicle of STZ (0.2 ml/kg body weight sodium citrate buffer, IP, single dose).

Subgroup Ic: Rats were treated with vehicle of exosomes, DKK1 and Wnt3a (0.2 ml phosphate buffer saline, single intravitreal injection).

Group II (DR group; n = 18): Diabetic rats which were further equally allocated to two subgroups:

Group IIa: Diabetic rats were sacrificed after 8 weeks to confirm histological changes of DR.

Group IIb (recovery group): Diabetic rats were sacrificed after 12 weeks.

Group III (DR + DKK1; n = 9): After 8 weeks of diabetes, rats were intravitreally injected with 3 µl of Recombinant Mouse Dkk-1 [15].

Group IV (DR + exosomes; n = 9): After 8 weeks of diabetes, rats

Table 1
Sequences for primers used.

Target genes	Primer Sequence 5' to 3'	Accession No
<i>VEGF</i>	CGGGCCTCTGAAACCATGAA GCTTTCTGCTCCCTTCTGT	NM_001110333.2
<i>c-Myc</i>	TGAAAAGAGCTCCTCGCGTT AAATAGGGCTGCACCGAGTC	NM_012603.2
<i>cyclin D1</i>	CCGGTCGTAGAGCGGAG CGGATGGTCTCCACTTCGCA	NM_171992.5
<i>ICAM-1</i>	TTTCAGTCCCATCCTGACC GGGAAGTACCCTGTGAGGTG	NM_012967.1
<i>VE-cadherin</i>	TGGGGACCCAATCTCATTGC GTCTTTGGTACCCACAGGCA	NM_001107407.1
<i>TNF-α</i>	CGTCAGCCGATTTGCCATT TCCCTCAGGGGTGTCCTTAG	NM_012675.3
<i>Nox2</i>	GTTTGGCGAAACCTCCTA CCTTCTGCTGAGATCGCCAA	NM_023965.1
<i>Nox4</i>	TGGCCAAGCAAGGGTTAAA TCCTAGGCCAACATCTGGT	NM_053524.1
<i>SOD1</i>	TGGCCGTAATATGGTGGTC GGGCAATCCCAATCACACCA	NM_017050.1
<i>SOD2</i>	CACCGAGGAGAAGTACCACG TGTGATTGATATGGCCCG	NM_017051.2
<i>GAPDH</i>	GCATCTTCTGTGAGTCC TACGGCCAATCCGTTACA	NM_017008.4
<i>U6</i>	CTCGCTTCGGCAGCACA AACGCTTCACGAATTTGCGT	[37]
miR-129-5p	ACACTCCTTTTTCGCTGGGCTTGC TGGTGTCGTGGAGTCG	[38]
miR-34a	GCCTGGCAGTGTCTTAGCT GTGCAGGGTCCGAGGTC	[39]

were injected intravitreally with MSC-exosomes in a single dose of 0.5 ml for each rat at a concentration (100 µg protein/ml) [30].

Group V (DR + Wnt3a; n = 9): After 8 weeks of diabetes, rats were intravitreally injected with 20 ng of recombinant Mouse Wnt3a.

Group VI (DR + exosomes + Wnt3a; n = 9): After 8 weeks of diabetes, rats were injected once with exosomes and single injection of Wnt3a [36], Fig. 1.

The intravitreal injection was performed using a 1.5 cm 33-gauge Hamilton needle (Hamilton Company, Reno, NV). The injection needle was angled to avoid hitting the lens. Each injected eye was treated topically post-injection with a polymyxin B sulfate ointment.

2.3. Sampling

At the end of the experimental period, rats were fasted for 12 h then anesthetized by intramuscular injection of ketamine (100 mg/kg) –xylazine (10 mg/kg). The rats were fixed on an operating table and vascular perfusion fixation was performed through the left ventricle. The eyeballs were then enucleated, the retina separated from the eyecup and dissected to be appropriately processed for histopathological examination [electron microscopy, staining with Hematoxylin and Eosin (H&E) and immunohistochemistry for iNOS, VEGF, GFAP and NF-κB]. In addition, retinal tissues were used for molecular analysis by Real Time PCR and Western blot. Fixation was performed by using 10% buffered formol saline for light microscopy or Glutaraldehyde (1%) for electron microscopy.

2.4. Gene expression profile

For RNA extraction from the retinal tissues, TRIzol (Invitrogen) was used following manufacturer's instructions. Sigma's mirPremier microRNA Isolation Kit was used for miRNA purification. Extracted RNA was tested for purity and RNA concentration was assayed using Nano-Drop 2000C spectrophotometer (Thermo Scientific, USA). RNA purity for all samples was > 1.9 A260/A280ratio. The integrity of RNA was then verified by loading on 2% agarose gel using a gel electrophoresis image (Gel Doc. BioRad) according to [34]. RNA was used for complementary

DNA (cDNA) synthesis using SensiFast cDNA synthesis kits (Sigma Bioline, UK) according to the manufacturer's instruction. NCode VILO miRNA cDNA Synthesis Kit (Invitrogen) was used for cDNA synthesis from miRNAs following the manufacturer's recommendations using a T100 Thermal Cycler (Bio-Rad, USA).

Quantitative PCR was performed according to [37] using Maxima SYBR Green/ROX qPCR master mix [2x] (Thermo Scientific, USA). Each PCR reaction consisted of 0.3 µmol L⁻¹ of each forward and reverse primer, 10 nmol L⁻¹/100 Nm ROX Solution, 500 ng per reaction of cDNA (except for NTC and cDNA control) and 12.5 µl Maxima SYBR Green qPCR Master Mix (Maxima SYBR Green qPCR, ThermoFisher Scientific). The mix was completed to a final volume of 25 µl with nuclease-free water. Primer pairs for selected target, miRNA and reference genes (*VEGF*, *c-Myc*, *Cyclin-D1*, *ICAM-1*, and *TNF-α*, *Nox2*, *Nox4*, *VE-cadherin*, *SOD1*, *SOD2*, *GAPDH*, miR-129-5p, miR-34a, U6) were purchased from Genwez (New Jersey, USA) (Table 1). The reaction was completed using a two-step protocol in AriaMx Real-Time PCR (Agilent Technologies, USA): initial denaturation for 10 min at 95 °C, then 40 cycles (15 s each) of denaturation at 95 °C followed by annealing/extension for 60 s at 60 °C. Following PCR, a melting curve protocol was performed by heating for 30 s at 95 °C then for 30 s at 65 °C and for 30 s at 95 °C. GAPDH was used as a housekeeping gene for normalization of the expression levels of target genes while the expression of miRNAs was normalized relative to U6 RNA as an internal housekeeping reference gene. The formula: $RQ = 2^{-\Delta\Delta Ct}$ was used to calculate relative gene expression ratios (RQ) between treated and control groups.

2.5. Assessment of SOD and NOX1 in retinal tissue homogenate

Retinal tissue was used for assessment of superoxide dismutase (SOD, ab65354, Abcam, Cambridge, UK) by colorimetric method and NADPH oxidase 1 (NOX1, E1408Ra) by ELISA method, following manufacturers' protocols.

2.6. Western blot

For exosome identification, western blot analysis for CD63, CD81 and CD83 antibodies were utilized (Table 1). RIPA buffer was used for isolation of protein from isolated exosomes. 20 ng of protein was loaded on 4–20% polyacrylamide gradient gels and separated by SDS-PAGE. The separated protein was blotted to PVDF membranes which were further blocked by incubation for 1 h in 5% nonfat dry milk. The membranes were then incubated overnight at 4 °C with primary antibodies (CD63, CD81, CD83 antibodies). β-actin was used as a loading control. The membranes were then washed two times with 1% TBST and further incubated for 2 h at room temperature with appropriate secondary antibodies. Another washing step was applied by washing the membrane twice with 1% TBST. Intensity of immunoreactivity was determined by densitometry to quantify the amounts of CD63, CD81, CD83. ChemiDoc MP imaging system (version 3) (BioRad, Hercules, CA, USA) was used for image analyses.

For Retina tissue western blot analysis, P-β-Catenin, β-Catenin, LRP6, PLRP6, GFAP, NF-κB and β-actin antibodies were employed (Table 1). Ice-cold 1X cell lysis buffer was prepared for protein extraction from retinal tissues. The buffer consisted of Tris (50 mmol, SRL, Mumbai, India), sodium chloride (150 mmol, Sigma Aldrich), sodium fluoride (1 mol, Fischer Scientific, Qualigens, Mumbai), EDTA (1 mmol, Fischer Scientific, New York), phenylmethylsulfonyl fluoride (2 mmol, Sigma-Aldrich), sodium dodecyl sulfate (0.1%, SDS; Fischer Scientific), Triton X-100 (1%, Sigma Aldrich) and protease inhibitor cocktail (4%, Roche Diagnostics, Mannheim, Germany). Whole retinas were minced and homogenized by passing through hypodermic needles (20 G, 22 G, and 26 G).

Produced cell lysates were agitated on ice for 30 min, and then supernatant was collected by centrifugation for 30 min at 21,000g. Folin-Lowry method was used for estimation of protein concentration using a

Table 2

List of antibodies used for western blot and immunohistochemistry with Host, Type, Dilutions, Catalog Number, Suppliers, and Analysis Type.

Antibody	Host	Type	Dilution	Cat. Number	Suppliers	Analysis Type
CD63	Rabbit	Polyclonal	1/1000	A5271	Abclonal	Western Blot
CD81	Rabbit	Monoclonal	1/1000	Ab109201	Abcam	Western Blot
CD83	Rabbit	Polyclonal	1/1000	PA5-96044	ThermoFisher Scientific	Western Blot
P- β - Catenin	Rabbit	Polyclonal	1/1000	#9561	Cell Signaling Technology	Western Blot
β - Catenin	Rabbit	Polyclonal	1/4000	Ab6302	Abcam	Western Blot
LRP6	Rabbit	Polyclonal	1/1000	#2560	Cell Signaling Technology	Western Blot
PLRP6	Rabbit	Polyclonal	1/500	Ab226758	Abcam	Western Blot
β -actin	Mouse	Monoclonal	1/1000	Ab8226	Abcam	Western Blot
iNOS	Rabbit	Monoclonal	1/20	Ab178945	Abcam	Immuno-histochemistry
VEGF	Rabbit	Monoclonal	1/250	Ab32152	Abcam	Immuno-histochemistry
GFAP	Rabbit	Polyclonal	1/5000	Ab7260	Abcam	Immuno-histochemistry
NF-kB	Rabbit	Polyclonal	1/100	Ab194726	Abcam	Immuno- histochemistry

spectrophotometer (Beckman Coulter Inc, Indianapolis, Indiana). Laemmli buffer was mixed and incubated with protein extracts for 10 min at 95 °C. Then, protein samples were loaded (50 μ g) on sodium dodecyl sulfate (SDS) polyacrylamide 10% and resolved by gel electrophoresis. The resolved protein was blotted onto polyvinylidene difluoride membrane (Amersham Biosciences, Bucks, United Kingdom). The blot was then blocked for non-specific reactions by incubation for 1 h at 4 °C in 5% nonfat dry milk (NFD) in 1% TBS with Tween 20. Following blocking, the membrane was kept for 2 h at 4 °C with primary antibodies against β catenin, P-b catenin, LRP6 and P-LRP6. Thereafter, the membrane was washed and then incubated for 2 h at room temperature with appropriate horseradish peroxidase-conjugated secondary antibody (1:5000, Millipore). Actin was used for normalization and was detected using secondary antibody (MAB1501, Millipore) at a 1:5000 dilutions.

Immunoreaction was visualized using Super Signal West Femto substrate (Thermo Scientific, Waltham, Massachusetts) on photographic films (Eastman Kodak Co, Rochester, New York). Housekeeping protein was detected after blot stripping by stripping buffer (62.5 mmol Tris, 2% DS, 100 mmol β -Mercaptoethanol) at 60 °C for 10 min. Densitometric analysis of the immunoblots was performed using Image analysis software on the Chemi Doc MP imaging system to quantify the amounts of β catenin, P-b catenin, LRP6 and P-LRP6 by total protein normalization.

2.7. Histopathological analysis

2.7.1. H&E staining

Retinal tissues were excised, fixed in buffered formol saline (10%). Fixed tissue specimens were used for preparation of 4–6- μ m-thick paraffin sections which were mounted on glass slides for hematoxylin and eosin (H&E), and positively charged slides for immunohistochemistry (IHC).

For H&E, fixed sections were dehydrated with successive concentrations of ethanol and washed twice in distilled water followed by staining with H&E stains. Finally, the histological sections were observed, analyzed and imaged by two blinded experienced investigators using light microscope (Leica DMR 3000; Leica Microsystem) [35].

2.7.2. Immunohistochemistry analysis

Paraffin sections were deparaffinized and hydrated. After blocking the endogenous activity of peroxidase using 10% hydrogen peroxide, the sections were incubated with primary antibodies against iNOS, VEGF Receptor 1, GFAP, and NF-kB (Table 2), using a concentration of 1–5 μ g/ml. Heat mediated antigen retrieval was performed before commencing with IHC staining protocol, (abcam, UK). Then, after washing with phosphate buffer, biotinylated goat anti-rabbit secondary antibody was applied. Slides incubated with labeled avidin–biotin peroxidase. Diaminobenzidine was used as chromogen for visualization of the site of

antibody binding which is converted into a brown precipitate by peroxidase [40].

For NF-Kb IHC quantitative assessment, immunoreactive score (IRS) was used. It provides a scale of 0–12 representing IRS index (0–1 = negative, 2–3 = mild, 4–8 = moderate, and 9–12 = strongly positive). IRS is obtained by multiplication between staining intensity grading (0–3) and positive cells proportion grading (0–4) and quantified using the QuPath program (0.1.2).

2.7.3. Morphometric study

Image-Pro Plus program version 6.0 (Media Cybernetics Inc., Bethesda, Maryland, USA) was used for calculation of the mean area % of iNOS, VEGF, GFAP and NF-kB. The mean area % for each marker was quantified for five images from five non-overlapping fields from each rat of each group.

2.7.4. Transmission electron microscopy study

Glutaraldehyde (1%) was used for vascular perfusion fixation through the left ventricle. Rat retinal tissues were then dissected and incubated in 0.1 M phosphate-buffered solution (PBS), pH 7.4 for 2 h at 4 °C, then washed three times (10 min each) with PBS. Samples were post fixed in 1% osmic acid for 30 min, and then washing was repeated with PBS three times (10 min each). Fixed specimens were dehydrated using ethyl alcohol solutions (ascending series) for 30 min at each concentration (30, 50, 70, 90%, and absolute alcohol). Dehydrated specimens were infiltrated for 1 h with acetone followed by embedding in Araldite 502 resin. Leica UCT ultra-microtome was used to cut the plastic molds into semi thin sections which were stained with 1% toluidine blue. Following semi thin sections examination, ultrathin sections were prepared (50–60 nm thick), treated with uranyl acetate for staining and then with lead citrate for counterstaining. The sections were further analyzed and photographed using electron microscope (JEOL-JEM-100 SX, Japan), electron microscope unit, Tanta University (10948426).

2.8. Ocular coherence tomography (OCT)

Retinal structure was analyzed using Spectral-domain optical coherence tomography (SD-OCT). The SD-OCT measurements were obtained with Spectralis Heidelberg retina angiography (HRA) + OCT device that was segmented with Spectralis viewing module software (Heidelberg Engineering Inc., Heidelberg, Germany). The software delivers high-resolution OCT images with a lateral resolution of 5.7 μ m/pix and provides 55-degree field of view. Automatic real-time registration was used with a mean of 100 scans at the exact same location. All scans had a quality index greater than 25 dB.

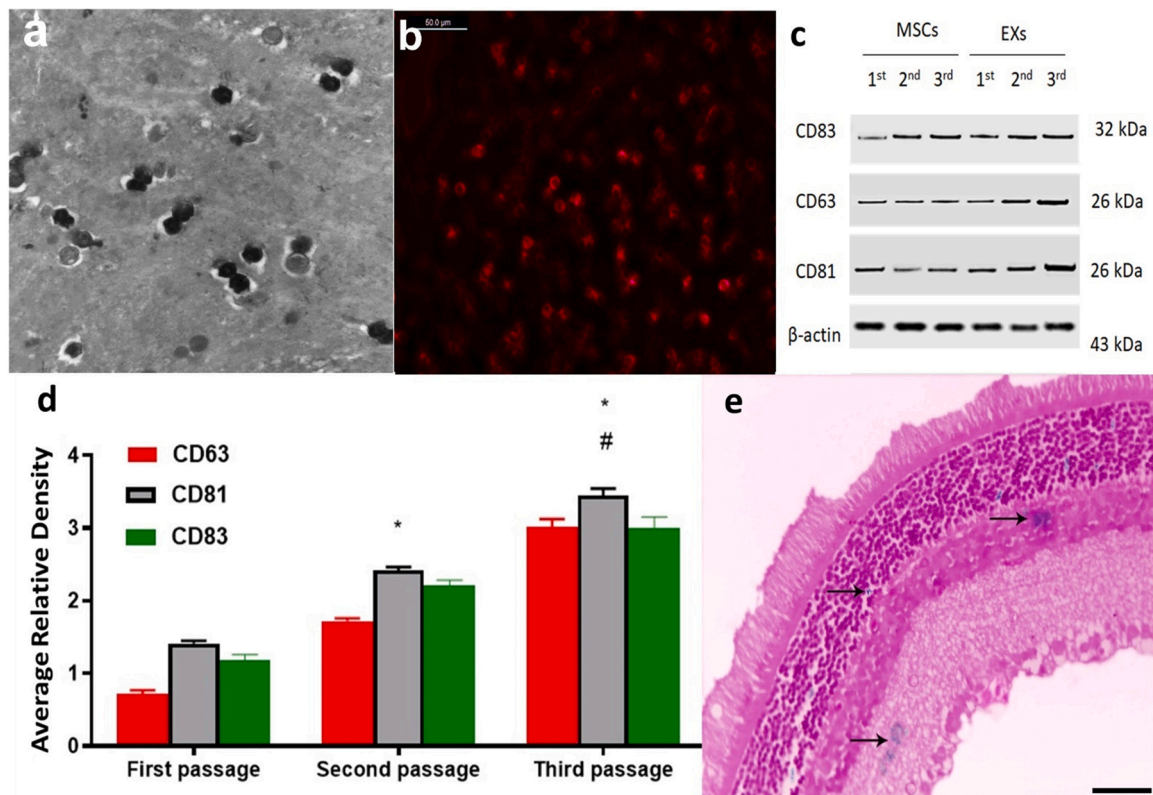


Fig. 2. (a) Ultrastructure of exosomes by TEM showing characteristic spheroid double-membrane bound morphology (arrows) of exosomes, they are heterogeneous in size with a diameter of 40–100 nm. Scale bar 100 nm (b) Detection of exosomes in retinal tissues by PKH26 under fluorescent microscopy. (c) Western blot analysis of exosomal specific markers (CD63, CD81, CD83) in three different passages. *significant compared to first passage at $p < 0.05$, ## significant compared to second passage at $p < 0.05$. Data are shown as mean \pm SE. (e) Prussian blue staining proved iron oxide particles stained blue in retinal tissues.

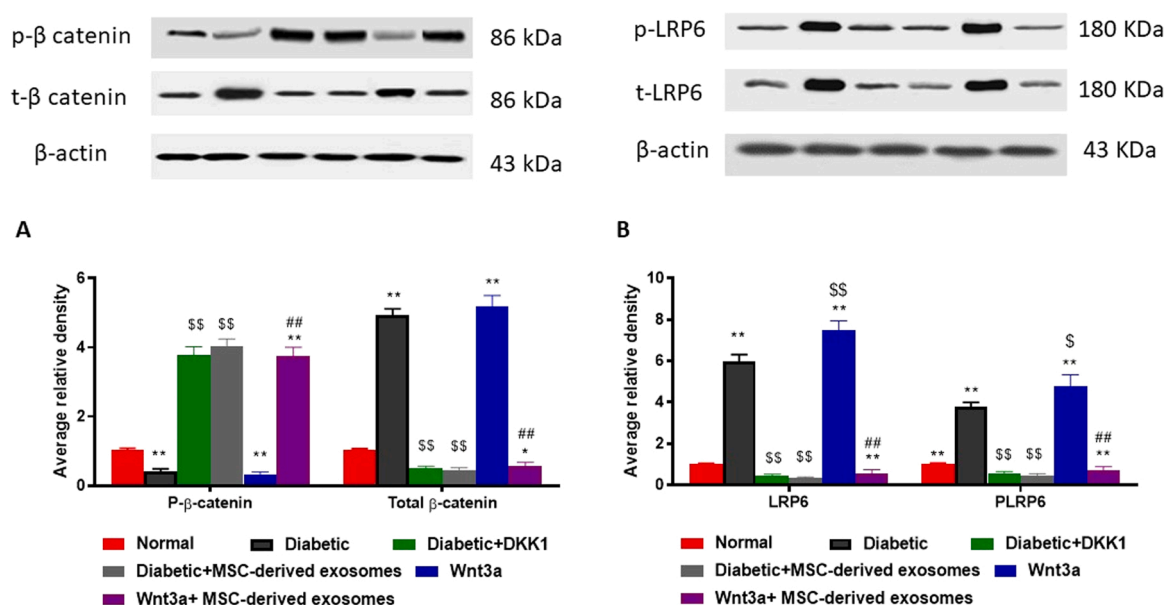


Fig. 3. Effect of BM MSC-derived exosomes intravitreal administration on wnt/b-catenin pathway in diabetic rats. MSC-derived exosomes were intravitreally injected to eight weeks' diabetic rats in a single dose of 0.5 ml for each rat at a concentration (100 μ g protein /ml) alone or in combination with wnt3a (20 ng). Additional group received DKK1 3 μ l. Western blot was used to evaluate average relative density of phosphorylated b-catenin and total b- catenin (A) LDL Receptor Related Protein 6 (LRP6) and Phospho-LRP6 (B) in retinal tissues of various experimental groups. * Represents significance in comparison with control group at $p < 0.05$, ** represents significance in comparison with control group at $p < 0.01$, \$ represents significance in comparison with diabetic group at $p < 0.05$, \$\$ represents significance in comparison with diabetic group at $p < 0.01$, ## represents significance in comparison with wnt3a group at $p < 0.01$. Data are expressed as mean \pm SE, (n = 6).

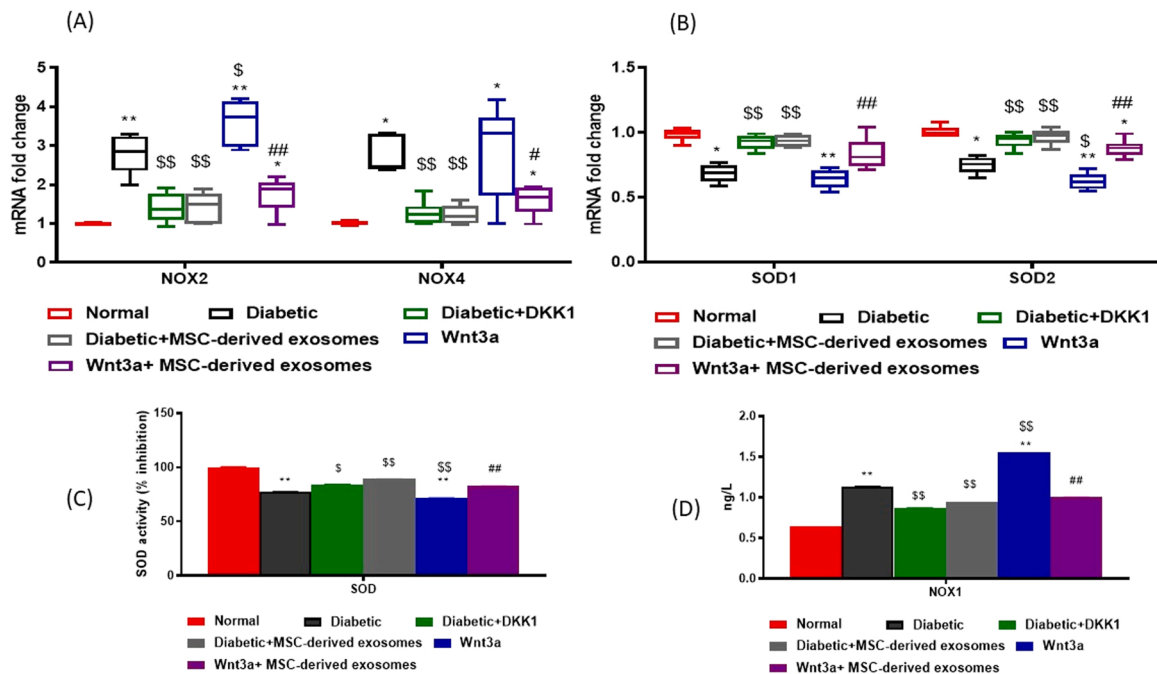


Fig. 4. Effect of BM MSC-derived exosomes intravitreal administration on wnt/b-catenin induced oxidative stress in diabetic rats. MSC-derived exosomes were intravitreally injected to eight weeks diabetic rats in a single dose of 0.5 ml for each rat at a concentration (100 µg protein /ml) alone or in combination with wnt3a (20 ng). A further group of diabetic rats received DKK1. RT-PCR was used to evaluate mRNA levels of NADPH oxidase 2 (*Nox2*) and *Nox4* (A), superoxide dismutase 1 (*SOD1*), (*SOD2*) in retinal tissues of various experimental groups (B). Data are expressed as median (maximum and minimum). SOD activity was assayed in retinal tissue by colorimetric assay (C), and NOX1 concentration was assayed by ELISA method (D). Data are expressed as mean±SE. * represents significance in comparison with control group at p<0.05, ** represents significance in comparison with control group at p<0.01, \$ represents significance in comparison with diabetic group at p<0.05, \$\$ represents significance in comparison with diabetic group at p<0.01, ## represents significance in comparison with wnt3a group at p<0.01, (n = 6).

2.9. Statistical analysis

Statistical software package SPSS for Windows (Version 16.0; SPSS Inc., Chicago, IL, USA) was used for performing statistical analysis. Differences between various experimental groups were evaluated using one-way Analysis of Variance (ANOVA; F) and Kruskal Wallis test (χ^2) for parametric and non-parametric data, respectively. Post-hoc analysis was then performed to detect differences in pairs. Parametric data were expressed as mean ± standard error (SE), non-parametric data were expressed as median (maximum and minimum) and a P-value < 0.05 was considered significant.

3. Results

3.1. Characterization of exosomes

Transmission electron microscopy demonstrated exosomes with characteristic spheroid double-membrane bound morphology with 40–120 nm diameter (Fig. 2a). Expression of exosome membrane markers CD63, CD81, and CD83 was confirmed in exosomes isolated from passages 1–3 (Fig. 2c&d). Increased expression of CD63, CD81 and CD83 correlated with passage number with significant differences noted between passages 1, 2, and 3.

The exosomes labelled with iron-oxide were observed in the retinal tissue under a light microscope after staining with Prussian blue (Fig. 2e). Also, under fluorescent microscopy exosomes labeled with PKH26 dye, a red fluorescence chromophore inserted into the lipid bilayers of exosomes, were incorporated in retinal tissues which became clearly visible (Fig. 2b).

3.2. MSC-derived exosomes blocked wnt/b-catenin pathway in diabetic retina

Dysregulated wnt/b-catenin signaling was observed in diabetic retina. This was indicated by significant increases in protein levels of total b-catenin, LRP6 and PLRP6 by 4.8-, 5.8-, 3.88-fold, respectively, accompanied by marked downregulation of phosphorylated b-catenin by about 0.6 fold in retinal tissue of diabetic compared to control groups. Administration of DKK1 blocked wnt/b catenin activation as demonstrated by a significant decrease in total b-catenin, LRP6, PLRP6 by about 0.9-, 0.85-, 0.92-fold, respectively accompanied by marked increase in phosphorylated b-catenin level in retinal tissue by 9.2-fold when compared to diabetic group. MSC-derived exosomes similarly blocked wnt/b catenin activation in diabetic retina, where retinal protein levels of total b-catenin, LRP6, PLRP6 were significantly reduced by approximately 0.9-, 0.87-, 0.94-fold respectively with significant upregulation of phosphorylated b-catenin level in retinal tissue by 0.99-fold when compared to diabetic group. In contrast, wnt3a administration triggered wnt/b-catenin activation in diabetic retina as shown by noticeable increase in total b-catenin, LRP6, PLRP6 protein levels by 1.05-, 1.2-, 1.2-fold, respectively, accompanied by decreased phosphorylated b-catenin level in retinal tissue by about 1.8-fold when compared to diabetic group. However, MSC-derived exosomes co-administration blocked this effect as manifested by decreased retinal protein levels of total b-catenin, activated b-catenin, LRP6, PLRP6 by approximately 0.89-, 0.85-, 0.92-, respectively, accompanied by marked increase in phosphorylated b-catenin level in retinal tissue by 11.2-fold when compared to wnt3a injected group, Fig. 3.

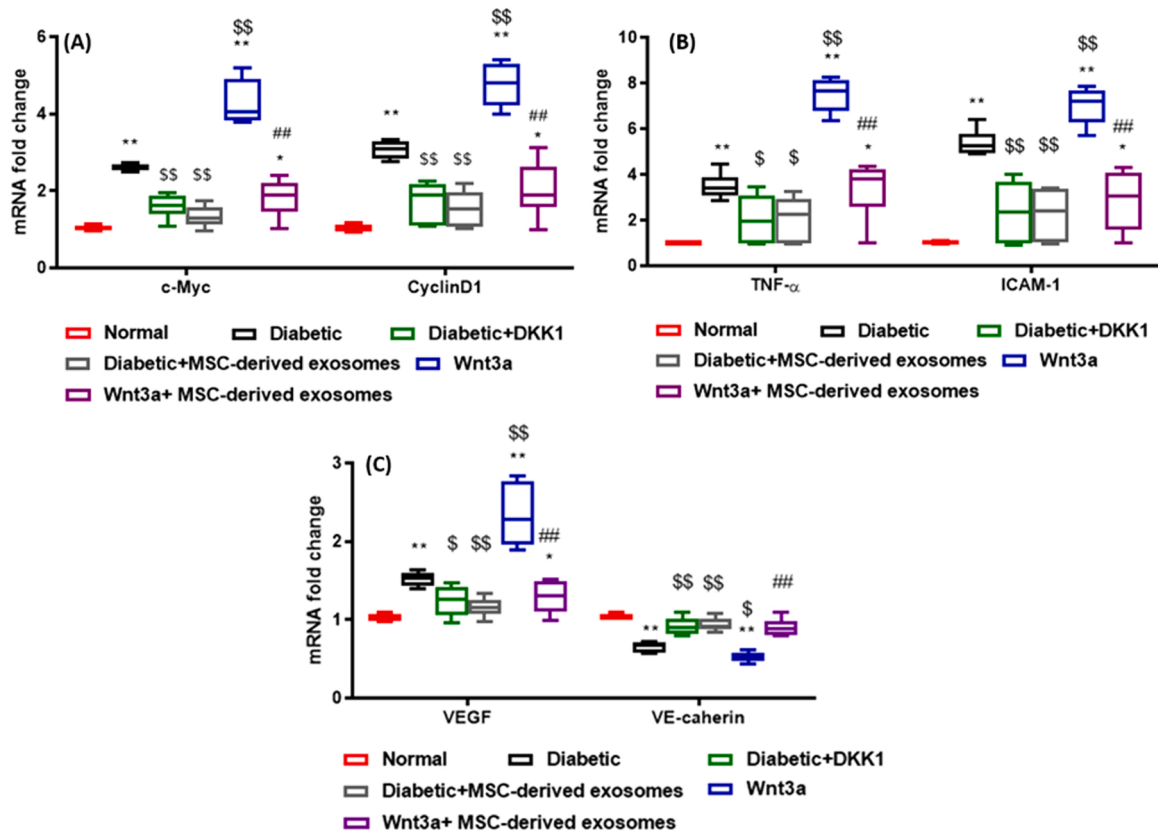


Fig. 5. Effect of BM MSC-derived exosomes intravitreal administration on wnt/b-catenin triggered inflammation in diabetic rats. MSC-derived exosomes were intravitreally injected to eight weeks’ diabetic rats in a single dose of 0.5 ml for each rat at a concentration (100 µg protein /ml) alone or in combination with wnt3a (20 ng). A further group of diabetic rats received DKK1. RT-PCR was used to evaluate mRNA levels of *c-Myc* and *CyclinD1* (A), tumor necrosis factor-α (*TNF-α*) and intercellular adhesion molecule-1 (*ICAM-1*) (B), vascular endothelial growth factor (*VEGF*) and vascular endothelial-cadherin (*VE-cadherin*) (C) in retinal tissues of various experimental groups. * represents significance in comparison with control group at p<0.05, ** represents significance in comparison with control group at p<0.01, \$ represents significance in comparison with diabetic group at p<0.05, \$\$ represents significance in comparison with diabetic group at p<0.01, ## represents significance in comparison with wnt3a group at p<0.01. Data are expressed as median (maximum and minimum), (n = 6).

3.3. MSC-derived exosomes ameliorated wnt/b-catenin-triggered oxidative stress in diabetic retina

Significant up-regulation of oxidative stress transcriptional markers were observed in diabetic retina with increased *Nox2* and *Nox4* (2.78-, 2.67-fold, respectively) and decreased *SOD1* and *SOD2* expression by 0.3- and 0.34- fold, respectively in diabetic group compared to normal control. Similarly, *SOD* activity was decreased by 22.7% and *NOX1* level was increased by 1.75-fold compared to normal control. Blockage of the wnt/b-catenin pathway via DKK1 intravitreal administration resulted in significant decreases in retinal mRNA levels of *Nox2* and *Nox4* by about 0.49- and 0.53- fold, respectively as well as restoration of *SOD1* and *SOD2* mRNA levels by 1.25- and 1.35- fold, respectively compared to diabetic group. This was accompanied by restoration of *SOD* activity by ~ 9% and a decrease in *NOX1* by 0.22- fold compared to diabetic group. Similarly, administration of MSC-derived exosomes resulted in marked downregulation of retinal *Nox2*, *Nox4* mRNA levels and *NOX1* protein levels by 0.49-, 0.55-, 0.22- fold, respectively, coupled to upregulation of *SOD1*, *SOD2* mRNA levels and *SOD* activity by 1.36-, 1.29- fold and 15% respectively, compared to diabetic group. On the other hand, stimulation of wnt/b-catenin pathway via wnt3a administration increased retinal *Nox2*, *Nox4* mRNA levels and *NOX1* concentration by 1.3- and 1.1-, 1.3- fold, respectively and decreased *SOD1*, *SOD2* mRNA and *SOD* activity by 0.06- and 0.16- fold and 7% respectively in injected diabetic rats compared to diabetic group. This effect was reversed by concomitant administration of MSC-exosomes with wnt3a to diabetic rats, where

rats in this group showed significant reduction in retinal *Nox2*, *Nox4* mRNA levels and *NOX1* protein by about 0.52-, 0.45-, 0.35-, fold, respectively in addition to significant up-regulation of *SOD1*, *SOD2* mRNA levels by 1.3- and 1.4- fold, respectively, and *SOD* activity by 15% compared to wnt3a injected group, Fig. 4.

3.4. MSC-derived exosomes suppressed wnt/b-catenin-induced inflammation in diabetic retina

Induction of diabetes was accompanied by prominent up-regulation of inflammatory markers in retinal tissues including mRNA levels of *c-Myc*, *cyclinD1*, *TNF-α*, *ICAM-1* compared to control group. In contrast, the DKK1 treated group showed marked reduction of *c-Myc*, *cyclinD1*, *TNF-α*, *ICAM-1* by 0.39-, 0.44-, 0.41-, 0.56- fold, respectively compared to diabetic group. Injection of MSC-derived exosomes produced similar effects as depicted by marked reduction of *c-Myc*, *cyclinD1*, *TNF-α*, and *ICAM-1* by 0.49-, 0.5-, 0.4- and 0.58- fold, respectively compared to diabetic group. In contrast, retinal inflammation was enhanced by wnt3a injection into diabetic rats where mRNA levels of *c-Myc*, *cyclinD1*, *TNF-α*, *ICAM-1* were markedly increased in retinal tissues by 1.6-, 1.5-, 2.2-, 1.3- fold, respectively compared to diabetic group. However, co-administration of MSC-derived exosomes altered this effect as indicated by significant upregulation of these inflammatory markers by about 0.58-, 0.57-, 0.55-, 0.59- fold, respectively in comparison with wnt3a injected group, Fig. 5.

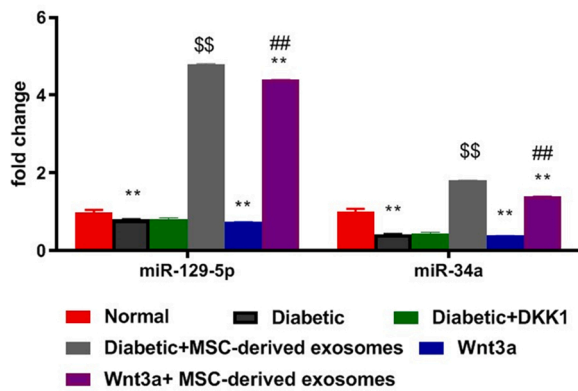


Fig. 6. Effect of BM MSC-derived exosomes intravitreal administration on miR-129-5 P& miR-34a expression levels. Quantitative analysis for relative expression of miR-129-5 P& miR-34a. * represents significance in comparison with control group at $p < 0.05$, ** represents significance in comparison with diabetic group at $p < 0.01$, \$ represents significance in comparison with diabetic group at $p < 0.05$, \$\$ represents significance in comparison with diabetic group at $p < 0.01$, ## represents significance in comparison with wnt3a group at $p < 0.01$. Data are expressed as mean \pm SE, (n = 6).

3.5. MSC-derived exosomes attenuated wnt/b-catenin-induced angiogenesis and vascular leakage in diabetic retina

VEGF is a major inflammatory and angiogenic factor regulated by the wnt/b-catenin pathway. Activated VEGF induces retinal neovascularization and vascular leakage in diabetic retina [41]. Further, VE-cadherin is an endothelial cell-specific adhesion molecule crucial for maintenance of retinal barrier integrity. VEGF induces disruption and degradation of VE-cadherin in DR [42]. To evaluate the impact of MSC-derived exosomes on wnt/b-catenin-induced angiogenesis and vascular leakage in diabetic retina, MSC-derived exosomes were administered to diabetic rats alone or in combination with wnt3a and compared to DKK1 administration. The diabetic group showed significantly increased retinal VEGF mRNA and protein by 1.4- and 3.7-fold, respectively, as well as downregulation of retinal VE-cadherin mRNA levels by 0.37- fold in comparison with control group. Blocking wnt/b-catenin by DKK1 significantly attenuated angiogenesis and barrier disruption as evident by marked suppression of retinal VEGF mRNA and protein levels by 0.18- and 0.48-fold, respectively with restoration of VE-cadherin mRNA levels by 1.4-fold compared to diabetic group. Similar results were observed in the MSC-derived exosomes treated group, where retinal VEGF mRNA and protein levels were significantly reduced by 0.24- and 0.54- fold, respectively. This was accompanied by a marked increase of retinal VE-cadherin mRNA level of 1.4-fold when compared to diabetic group. On the other hand, retinal VEGF mRNA and protein levels were significantly increased by wnt3a administration by 1.5, 1.73, fold, respectively in comparison to the diabetic group. Additionally, retinal VE-cadherin mRNA levels were markedly decreased by about 0.2-fold. Conversely, co-administration of MSC-derived exosomes attenuated angiogenesis and barrier disruption as demonstrated by significant reduction in retinal VEGF mRNA and protein levels by approximately 0.45- and 0.6- fold, respectively accompanied by marked increase in retinal VE-cadherin mRNA level by 1.7-fold in comparison with wnt3a injected group, Fig. 5.

3.6. MSC derived exosomes are associated with elevated miR-129-5 P and miR-34a

Retinal tissue from the diabetic group displayed significant decreases in miR-129-5 P and miR-34a expression by 0.8- and 0.42-fold, respectively, when compared to control group. Expression levels of miR-129-5 P and miR-34a in the DKK1 treated group were no different to the

control group. MSC-derived exosomes administration resulted in significantly increased expression of both miR-129-5 P and miR-34a by 4.8- and 1.8-fold, respectively, when compared to the diabetic group. In contrast, Wnt3a administration decreased expression of both miR-129-5 P and miR-34a by 0.26- and 0.61- fold, respectively, when compared to the control group. However, this effect was blocked by co-administration of MSC-derived exosomes, resulting in increased expression of miR-129-5 P and miR-34a by 4.4- and 1.4-fold, respectively, when compared to either control group or Wnt3a injected group, Fig. 6.

3.7. Histological findings underlying role of Wnt/b-catenin in diabetic retinopathy treated with MSC derived exosomes

No histological differences were observed upon examination of retinal sections from the control subgroups. Therefore, the results of subgroup Ia were used to represent the control group.

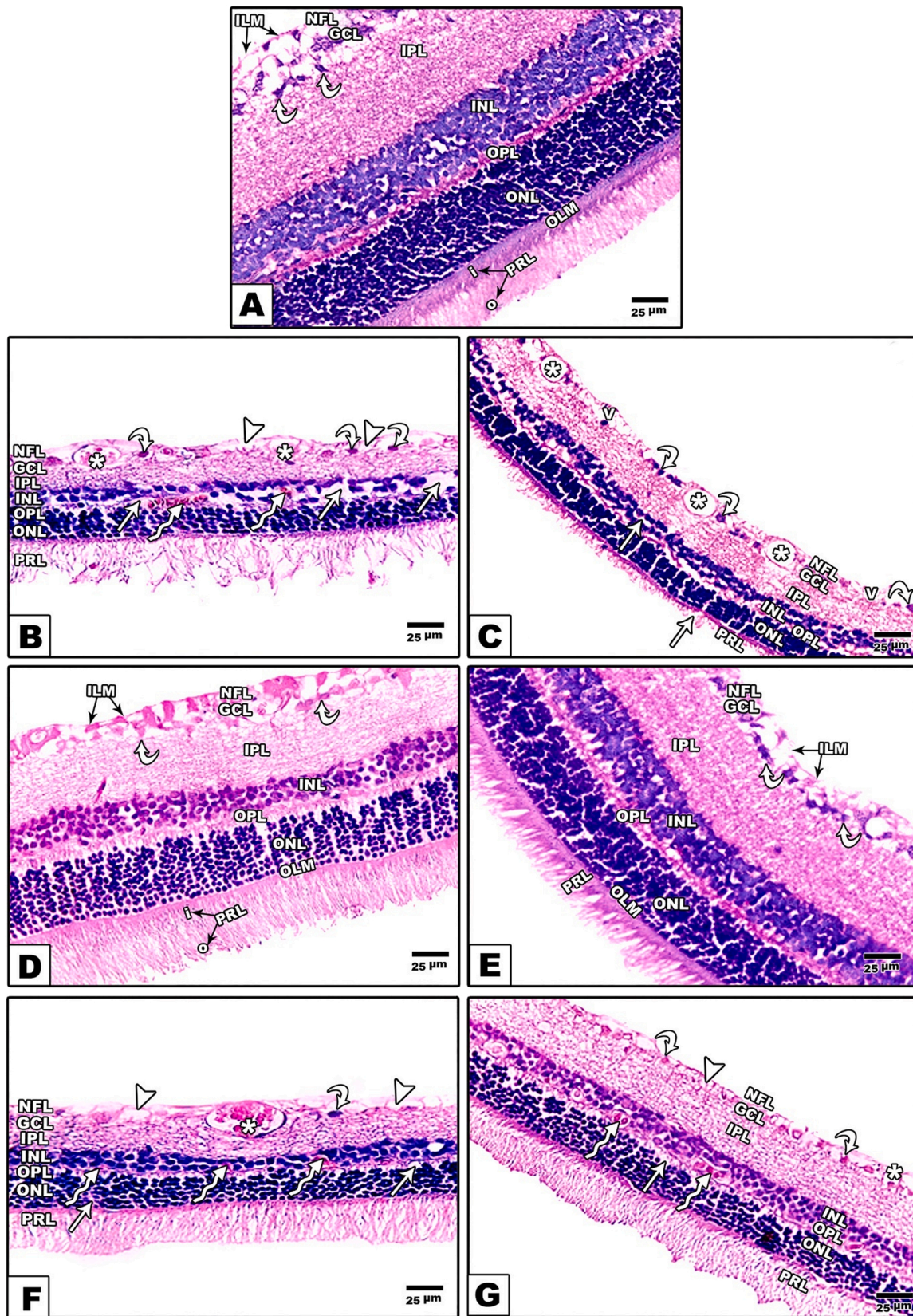
3.7.1. H&E results

Group I (control group) revealed a normal retinal histology consists of 10 layers organized from outward to inward: retinal pigment epithelial (RPE) layer, photoreceptor layer (PRL), outer limiting membrane (OLM), outer nuclear layer (ONL), outer plexiform layer (OPL), inner nuclear layer (INL), inner plexiform layer (IPL), ganglionic cell layer (GCL), nerve fiber layer (NFL) and inner limiting membrane (ILM), Fig. 7a. **DR group (group IIa)** revealed decreased retinal thickness, small nuclei and extensive clear zones around the shrunken nuclei in GC associated with dilated and congested blood capillaries. INL verified broadening of intercellular spaces with vacuolation, eosinophilic necrotic material, and congested blood capillaries invading the OPL. Focal vacuolation and broadening of intercellular spaces in the ONL with atrophied photoreceptor layer were also observed, Fig. 7b. The recovery group (group IIb) revealed diminished retinal thickness with darkly stained small pyknotic nuclei of GCs with some large vacuolation. The nuclei of the INL and outer ONL were small and darkly stained. Multiple dilated new blood vessels were present in the NFL and the GCL. Widening of intercellular spaces between the cells of the ONL with atrophied photoreceptor layer was established, Fig. 7c. The DKK1 treated group (group III) revealed retinal tissues structure near normal except for few clear zones around nuclei of ganglionic cells and few focal broadening of intercellular spaces among the cells of the INL and ONL, Fig. 7d. The exosome treated group (group IV) revealed increased retinal thickness with near normal histological structure of retinal tissues, Fig. 7e. The Wnt3a treated group (group V) revealed the same histopathological changes as the DR group, Fig. 7f. Wnt3a and exosomes (**group VI**) showed DR histopathological alteration enhanced with enlarged retinal thickness and few blood capillaries in INL invading the IPL, Fig. 7g.

3.7.2. Immunohistochemistry results

3.7.2.1. iNOS immunohistochemistry. Retinas of control groups (group I) showed no immunoreactivity for iNOS, Fig. 8a, while retinal tissues of DR groups (group IIa, IIb) and Wnt3a treated group (Group V) revealed strong positive cytoplasmic and nuclear iNOS immunoreactivity in GCL and INL when compared to control group, Fig. 8b, c, f. DKK1 treated groups (group III) and exosome treated groups (Group IV) showed minimal cytoplasmic iNOS immunoreactivity within the GCL and INL when compared to control group, Fig. 8d, e. Group VI where Wnt3a was added in combination with exosomes revealed mild positive cytoplasmic iNOS immunoreactivity of GCL and INL, Fig. 8g.

3.7.2.2. VEGF immunohistochemistry. The retinas of control groups (group I) showed weak immunoreactivity for VEGF, Fig. 9a. While retinal tissues of DR groups (group IIa and IIb) and Wnt3a treated group



(caption on next page)

Fig. 7. Representative photomicrographs of hematoxylin and eosin-stained sections from retinal tissues. (A): Group I (control group) revealed that normal retinal layers; the photoreceptor layer (PRL) with outer segments (o) and inner segments (i) of rods and cones, the outer limiting membrane (OLM), the outer nuclear layer (ONL), the outer plexiform layer (OPL), the inner nuclear layer (INL), the inner plexiform (IPL), the ganglion cell layer (GCL) with large vesicular nuclei (curved arrows), the nerve fiber layer (NFL) and the inner limiting membrane (ILM). (B&F): Group IIa and V: displayed apparent decrease in retinal thickness. The ganglion cells revealed shrunken nuclei (curved arrows), wide clear areas (arrow heads) and large congested blood vessels (star) in-between. Focal widening of intercellular spaces of the INL and ONL (straight arrows) with multiple congested blood vessels (wavy arrows) in the (INL). (C): Group IIb (recovery group): displayed apparent marked reduction in retinal thickness. The Ganglion cells revealed pyknotic nuclei (curved arrow) and some vacuolation (v). Multiple dilated blood vessels (star) in the NFL and GCL can be seen. The INL & ONL showed wide intercellular spaces (straight arrow). (D): Group III (DR+DKK1 group): displayed apparently increased retinal thickness, with more regularly arranged layers. Some ganglion cells had euchromatic nuclei (curved arrow). Notice; the slightly decreased intercellular spaces between the cells of INL and ONL. (E): Group IV (DR+ exosomes): displayed nearly normal retinal histological architecture. Ganglion cells showing vesicular nuclei (curved arrow). (G): Group VI (DR+ Wnt3a+ exosomes group): some ganglion cells showed darkly stained nuclei (curved arrow) and clear areas in-between (arrow head). Some blood vessel appeared in the GCL (star) and INL (curved arrow). Focal widening of intercellular spaces between the cells of the ONL (straight arrow).

(Group V) revealed positive VEGF immunoreactivity in NFL, GCL, INL and OPL when compared to control group, Fig. 8b, c, and f. DKK1 treated groups (group III) and exosome treated groups (Group IV) showed minimal VEGF immunoreactivity within the NFL, GCL, INL and OPL when compared to control group, Fig. 8d and e. Group VI (Wnt3a and exosomes) revealed mild positive VEGF immunoreactivity in NFL, GCL, INL and OPL, Fig. 8g.

3.8. GFAP immunohistochemistry

Control group retinas (group I) showed weak immunoreactivity for GFAP adjacent to ILM in NFL and GCL while Müller cell processes were not stained, Fig. 10a. Retinal tissues of DR groups (Groups IIa and IIb) and Wnt3a treated group (Group V) revealed strongly positive GFAP immunoreactivity in NFL and GCL, which was more prominent around blood capillaries in the innermost layers of the retina. Müller cell processes which prolonged radially all over the retina displayed moderate positivity of GFAP immunoreactivity, Fig. 10b, c, and f. DKK1 treated, Group III and exosome treated group Group IV showed minimal GFAP immunoreactivity within the Muller cell end feet at ILM, Fig. 10d and e. While Group VI (Wnt3a and exosomes) revealed mildly positive GFAP immunoreactivity of Müller cell bodies and their processes. Fig. 10g.

3.9. NF- κ B immunohistochemistry

Localized NF- κ B immunostaining was detected in the cytoplasm and/or nucleus of cellular components in retinal neurons, glial cells, vascular ECs, and intravascular leukocytes. Cytoplasmic NF- κ B p65 expression represented an inactive protein state, while NF- κ B expression in the nucleus represented an active state.

The retinas of control groups (group I) showed no immunoreactivity for NF- κ B P65, Fig. 11a. Retinal tissues of DR groups (groups IIa and IIb) and Wnt3a treated group (Group V) revealed strong positive cytoplasmic NF- κ B P65 immunoreactivity in GCL and INL when compared to control group, Fig. 11b, c, and f. DKK1 treated groups (group III) and exosome treated groups (Group IV) showed minimal cytoplasmic NF- κ B P65 immunoreactivity within the GCL and INL when compared to control group, Fig. 11d and e. While, group VI, where Wnt3a was added with exosomes revealed mild positive cytoplasmic NF- κ B immunoreactivity of GCL and INL, Fig. 11g.

3.9.1. Morphometric study

The mean area percentage of iNOS, VEGF, NF- κ B and GFAP immunoreactivity for all groups are presented in, Fig. 8h, 9h, 10h and 11h, respectively. The DR groups (group IIa and IIb) and Wnt3a group (group V) showed a significant increase ($P < 0.05$) in the mean area percentage of iNOS, VEGF, NF- κ B and GFAP immunoreactivity compared to the control group. Furthermore, administration of DKK1 (group III) and exosomes (group IV) caused a significant decrease ($P < 0.05$) in the mean area percentage of iNOS, VEGF, NF- κ B and GFAP immunoreactivity to near control group. Wnt3a and exosomes (group VI), displayed non-significant increases in iNOS, VEGF, NF- κ B and GFAP immunoreactivity.

3.9.2. Ultrastructure examination of retinal tissues

3.9.2.1. Retinal Pigment Epithelial (RPE) cells and photoreceptors outer segments (POS).

RPE were resting on Bruch's membrane with basal mitochondria, large euchromatic oval nucleus, and long apical microvilli adjoining the POS. POS displayed straight and elongated structures. Parallel lamellar structures of the outer segment of photoreceptors were observed, Fig. 12a. DR group (group IIa) displayed RPE with broadly destructed apical microvilli, numerous large phagosomes and karyolytic nucleus. POS were vacuolated and disorganized with loss of the regular alignment of their lamellar disc membranes. There were extensive regions of complete loss of POS, Fig. 12b. Moreover, the recovery group (group IIb) RPE had vacuolated cytoplasm, shrunken nuclei with heterochromatin, large phagosomes, and distorted apical microvilli. POS were shrunken and distorted. There were areas occupied with debris. Projected some photoreceptors nuclei into the area of the outer segments might be perceived, Fig. 12c. DKK1 group (group III) displayed RPE resting on Bruch's membrane with apical microvilli and with large oval heterochromatic nuclei. POS were slightly detached in some instances and while some segments had a regular lamellar appearance, others displayed vacuolation, Fig. 12d. The exosomes treated group (group IV) displayed broadly normal RPE resting on Bruch's membrane and separating it from the Choriocapillaris layer. RPE had numerous long apical microvilli enclosing the outer segments and large oval heterochromatic nuclei. The POS had lamellar membranous discs Fig. 12e. In DR treated with Wnt3a (group V), the RPE had broadly destructed apical microvilli, numerous large phagosomes, and karyolytic nucleus. POS were vacuolated and disorganized with loss of regular alignment of their lamellar disc membranes. There were extensive regions of complete loss of POS, Fig. 12f. Wnt3a and exosomes in group VI had RPE resting on distorted Bruch's membrane in small areas while the rest of membrane was continuous and had large oval nuclei with many fragmented apical microvilli. Some POS had a regular lamellar appearance while some showed loss of typical orientation of their lamellar disc membranes with vacuolations and a few zones had loss of POS, Fig. 12g.

3.9.2.2. The ultrastructure of Ganglion cell layer (GCL).

Control group (group I) displayed GCs had uniformly staining nucleoplasm and rounded large euchromatic nuclei with prominent nucleoli, few mitochondria, RER, and scattered ribosomes. GC axons arose from a portion of the axon hillock, Fig. 13a. DR (group IIa) showed GCs with vacuolated cytoplasm and indented nuclei displaying convoluted sinuses with zones of electron-dense heterochromatin. Swollen mitochondria with destructed cristae and reduced matrix density can be observed, Fig. 13b. Moreover, in group IIb, the GCs showed a highly rarefied cytoplasm with large vacuoles. The small shrunken irregular heterochromatic nucleus (N) with irregular outlines was vacuolated with a slightly dilated disrupted nuclear envelope. The inner limiting membrane seemed abnormal, and the inner plexiform layer displayed destructed axons, Fig. 13c. In DKK1 (group III), the GCs had large euchromatic nuclei, and some swollen mitochondria with destructed cristae, Fig. 13d. The exosomes treated group (group IV) displayed near normal GCs with a cytoplasm having numerous ribosomes, slightly swollen mitochondria,

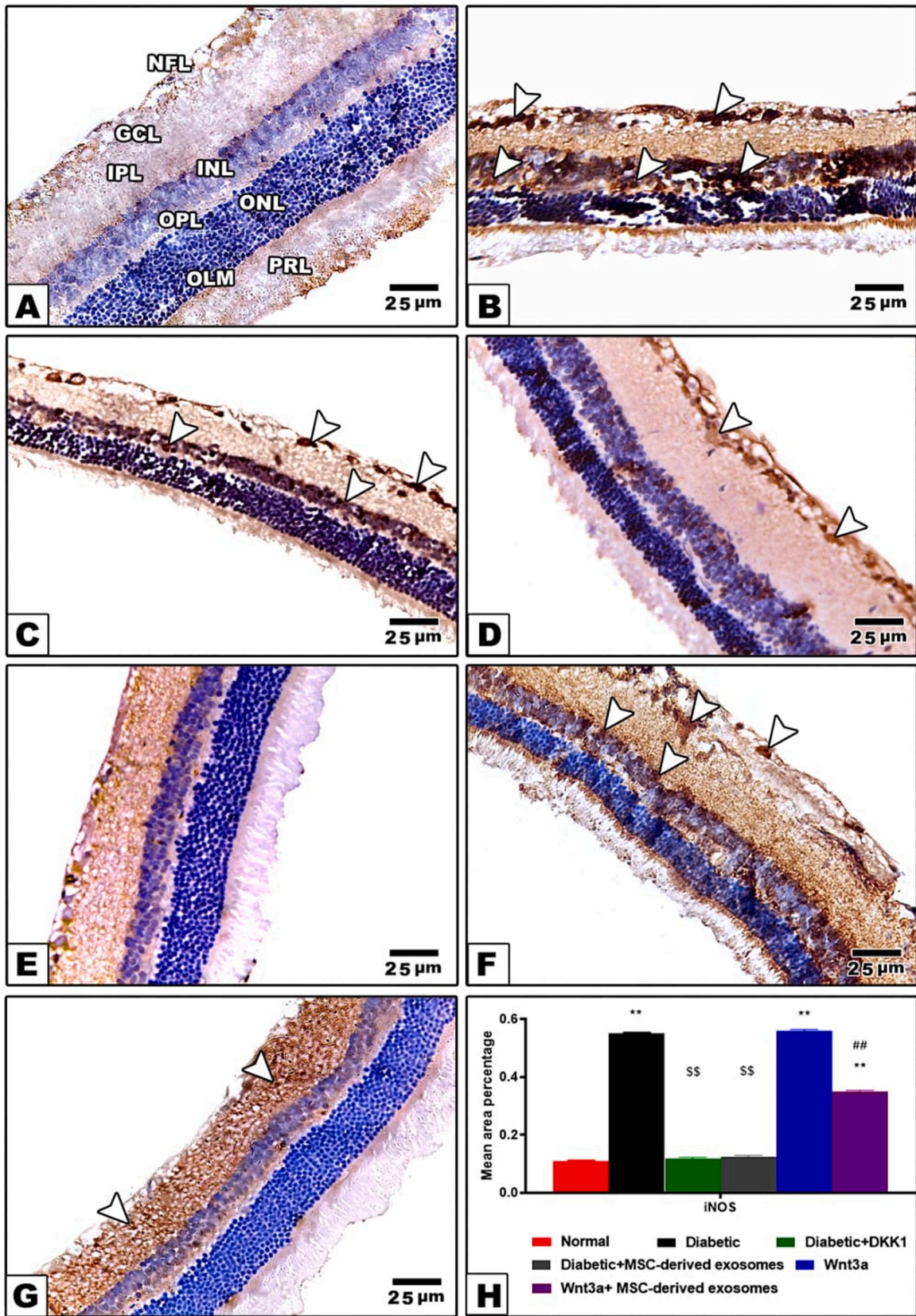


Fig. 8. Representative photomicrographs of iNOS immuno-stained sections from retinal tissues. (A) Control groups (group I) showed no immunoreactivity for iNOS. (B, C, and F): Groups IIa, IIb and Wnt3a revealed strong positive cytoplasmic iNOS immunoreactivity in GCL and INL. (D and E): Groups III and IV minimal cytoplasmic iNOS immunoreactivity within the GCL and INL. (G): Group VI revealed mild positive cytoplasmic iNOS immunoreactivity of GCL and INL. (H): Histogram representing the mean area percentage of iNOS immuno-reaction in all experimental groups. * Represents significance in comparison with control group at $p < 0.05$, ** represents significance in comparison with control group at $p < 0.01$, \$ represents significance in comparison with diabetic group at $p < 0.05$, \$\$ represents

significance in comparison with diabetic group at $p < 0.01$, ## represents significance in comparison with wnt3a group at $p < 0.01$. Data are expressed as mean \pm SE, (n = 6).

slightly dilated RER, and large oval euchromatic nuclei. GCs axons arose from a portion of the axon hillock, Fig. 13e. Group V (Wnt3a group) showed a degenerated ganglion cell with large nucleus, irregular nuclear envelope, areas of heterochromatin, swollen mitochondria with disintegrated cristae, and decreased matrix density, Fig. 13f. In Wnt3a and exosomes (group VI), the GCs displayed some swollen mitochondria with destructed cristae, Fig. 13g.

3.10. Fundus examination and Optical coherence tomography (OCT)

Control group (group I) displayed normal retinal appearance, optic nerve head and vasculature upon fundus examination. OCT scan of the retinal layers showed normal appearance and thickness of all the retinal layers. Fundus examination of DR group (group II) showed obscuration of the retinal appearance due to vitreous hemorrhage and venous beading (irregular dilatation of veins). OCT scan of the retinal layers shows irregular appearance and reduction of all the retinal layers thickness due to neurological degeneration. In DKK1 (group III), fundus examination showed normal retinal appearance, optic nerve head and vasculature. OCT scan of the retinal layers shows within normal appearance and reduction of the inner retinal layers thickness. The exosomes treated group (group IV) displayed normal retinal appearance, optic nerve head and vasculature in fundus examination. OCT scan of the retinal layers shows within normal appearance and thickness of all the retinal layers. Fundus photo of Group V (Wnt3a group) retinal rat shows obscuration of the retinal appearance due to vitreous hemorrhage and attenuation of the retinal vasculature. OCT scan of the retinal layers shows irregular appearance and reduction of all the retinal layers thickness due to neurological degeneration. In Wnt3a and exosomes (group VI), fundus photo of retinal rat shows obscuration of the retinal appearance due to vitreous hemorrhage and attenuation of the retinal vasculature. OCT scan of the retinal layers shows: irregular appearance and reduction of all the retinal layers thickness due to neurological degeneration, Fig. 14.

4. Discussion

DR is considered as one of the most serious complications of diabetes mellitus [43]. Hyperglycemia and hypoxia are the leading pathogenic factors causing retinal oxidative stress, inflammation, and microvascular injuries leading to blood-retinal barrier destruction, capillary failure and retinal ischemia with subsequent vision diminution and even blindness [44–46].

Recent studies have revealed that the Wnt/b-catenin signaling pathway is stimulated during pathogenesis of DR leading to inflammation, microvascular damage and retinal vascular leakage [47,48]. Recent reports indicate b-catenin accumulation and nuclear translocation in high glucose and hypoxia exposed in vitro cultured retinal endothelial cells [49]. Moreover, the canonical Wnt signaling pathway has been reported to be increased in retinal sections of patients with DR when compared to healthy non-diabetic controls [50]. Furthermore, expressional levels of b-catenin and LRP5/6 in retinal tissues are up-regulated in STZ-induced diabetic rats as well as oxygen-induced retinopathy [15].

These observations are consistent with the current study where the STZ induced diabetic rat model (group II) revealed significant upregulation of phosphorylated and total LRP6 that associated with significant upregulation of total b-catenin levels, with down regulation of phosphorylated b-catenin. These molecular changes were confirmed by histopathology in the form of reduced retinal thickness, signs of degenerated cells (RPE, ONL, INL and GCL), and congested dilated new blood capillaries. These outcomes are consistent with other reports [51,

52].

Dysregulation of Wnt signaling is linked with unbalanced oxidative stress, inflammation, and pathological angiogenesis that contribute to the pathogenesis of DR [41]. So, in the current study, we explored three underlying mechanisms of DR and their relation to Wnt/b-catenin.

The DR group showed significant upregulation of *Nox2*, *Nox4* and *Nox1*, downregulation of *SOD1* and *SOD2* mRNA, reduced SOD activity and increased iNOS immune-reaction. Recent reports have detailed that *Nox2* and *Nox4* are expressed abundantly in vascular endothelial cells, are considered as a chief source of vascular ROS production [53–55], and responsible for blood-retinal barrier dysfunction and retinal neovascularization in ischemic and DR [56,57]. Further, retinal SOD activity is decreased in DR compromising antioxidant defense capability and aggravating oxidative damages [58].

The Wnt/b-catenin cascade is suggested to be sensitive to activation by redox signaling. Mechanistically this is proposed to be a result of Nox1-derived ROS initiated oxidative-inactivation of the NRX and dissociation of NRX and Dvl, accelerating the activation of Wnt/b-catenin signaling [59,60]. *Nox4* overexpression increased LRP6 phosphorylation of; in contrast, knockdown of *Nox4* reduced HG-induced LRP6 phosphorylation, signifying a pivotal role of *Nox4*-derived ROS in Wnt/b-catenin activation [61]. Further, SOD transcriptional down-regulation via Wnt/b-catenin signaling cascade was concomitant with a previous study indicating that SOD activity was dramatically reduced via Wnt3a [62]. Taken together, in diabetic retina, hyperglycemia caused upregulation of Nox, increased ROS production, and activated Wnt/b-catenin concomitant with downregulation of SOD expression and activity and an increased retinal ROS burden.

In the current study we explored the role of canonical Wnt signaling in retinal angiogenesis. Significant upregulation of *VE cadherin* and *VEGF* mRNA levels. This was associated with vitreous hemorrhage and venous beading in fundus examination. *VEGF* is a recognized downstream target of canonical Wnt signaling [63]. With a significant function in new retinal blood vessels formation involved in pathogenesis of DR, *VEGF* levels in vitreous fluid and aqueous humor of DR patients correlate with DR severity [64]. Recent studies demonstrated up-regulation of LRP5 and Fzd-4 in a DR model while LRP5 loss suppressed pathological neovascularization in DR, signifying that Wnt signaling plays a potential role in control of pathological neovascularization within DR models [7].

Canonical Wnt signaling controls blood-retina barrier (BRB) integrity [65] via regulation of endothelial cell proliferation and maintaining vessel stability throughout vascular formation [66–68]. In DR, b-catenin overexpression causes BRB disruption through a dysregulated adhesive attachment, particularly the interaction among pericytes and retinal microvascular endothelial cells. Consistent with this is the observation that b-catenin activity is related to dysfunction and loss of pericytes confirming that the Wnt/b-catenin pathway exerts a crucial role in BRB integrity [69].

The DR group showed upregulation of *c-Myc*, *Cyclin-D1*, *ICAM-1*, and *TNF- α* with significantly increased NF κ B and GFAP protein. Retinal inflammation plays crucial role in vascular leakage leading to macular edema and neovascularization (NV). Recent studies revealed that *c-Myc* knock-down caused DR improvement via hastening the release of retinal Müller cell-derived pro-inflammatory cytokines. Additionally, *c-Myc* played a role in angiogenesis of endothelial cells and promoted retinal pigment epithelial cell proliferation [70].

ICAM-1 overexpression in diabetic retina triggers leukostasis which contributes to local ischemia and capillary non-perfusion causing *VEGF* overexpression [71,72]. Levels of *ICAM-1* were significantly higher in the vitreous from patients with DR [73,74]. Wnt/b-catenin signaling regulates the expression of pro-inflammatory and pro-angiogenic factors

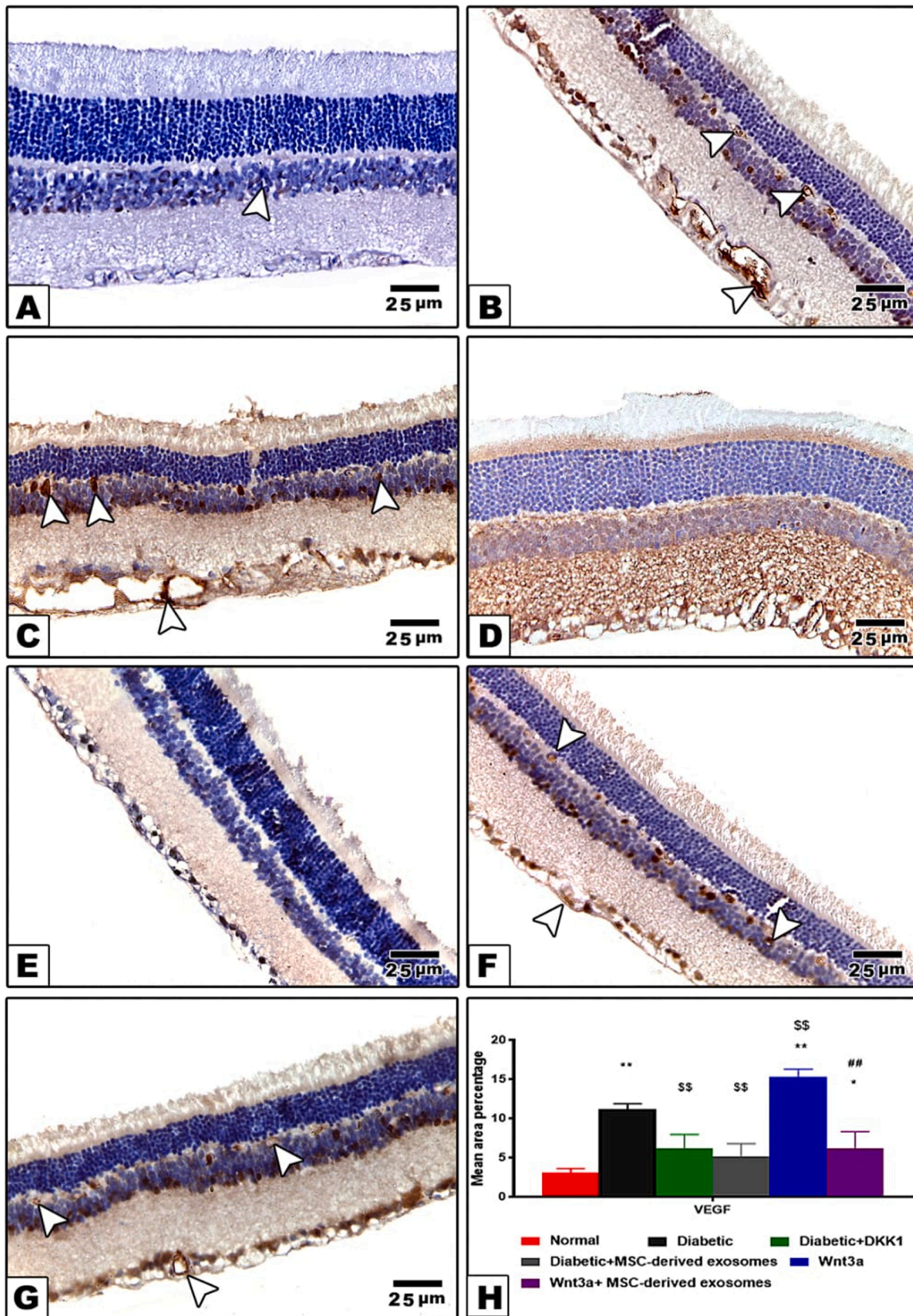


Fig. 9. VEGF immuno-stained retinal tissues. (A) Control groups (group I) showed weak immunoreactivity for VEGF. (B, C, and F): Groups Iia, Iib, and V revealed strongly positive VEGF immunoreactivity in NFL, GCL, INL, and OPL. (D and E): Groups III and IV showed minimal VEGF immunoreactivity within the NFL, GCL, INL and OPL. (G): Group VI revealed mild positive VEGF immunoreactivity of NFL, GCL, INL and OPL. (H): Histogram representing the mean area percentage of VEGF immuno-reaction in all experimental groups. * represents significance in comparison with control group at $p < 0.05$, ** represents significance in comparison with control group at $p < 0.01$, \$ represents significance in comparison with diabetic group at $p < 0.05$, \$\$ represents significance in comparison with diabetic group at $p < 0.01$, ## represents significance in comparison with wnt3a group at $p < 0.01$. Data are expressed as mean \pm SE, (n = 6).

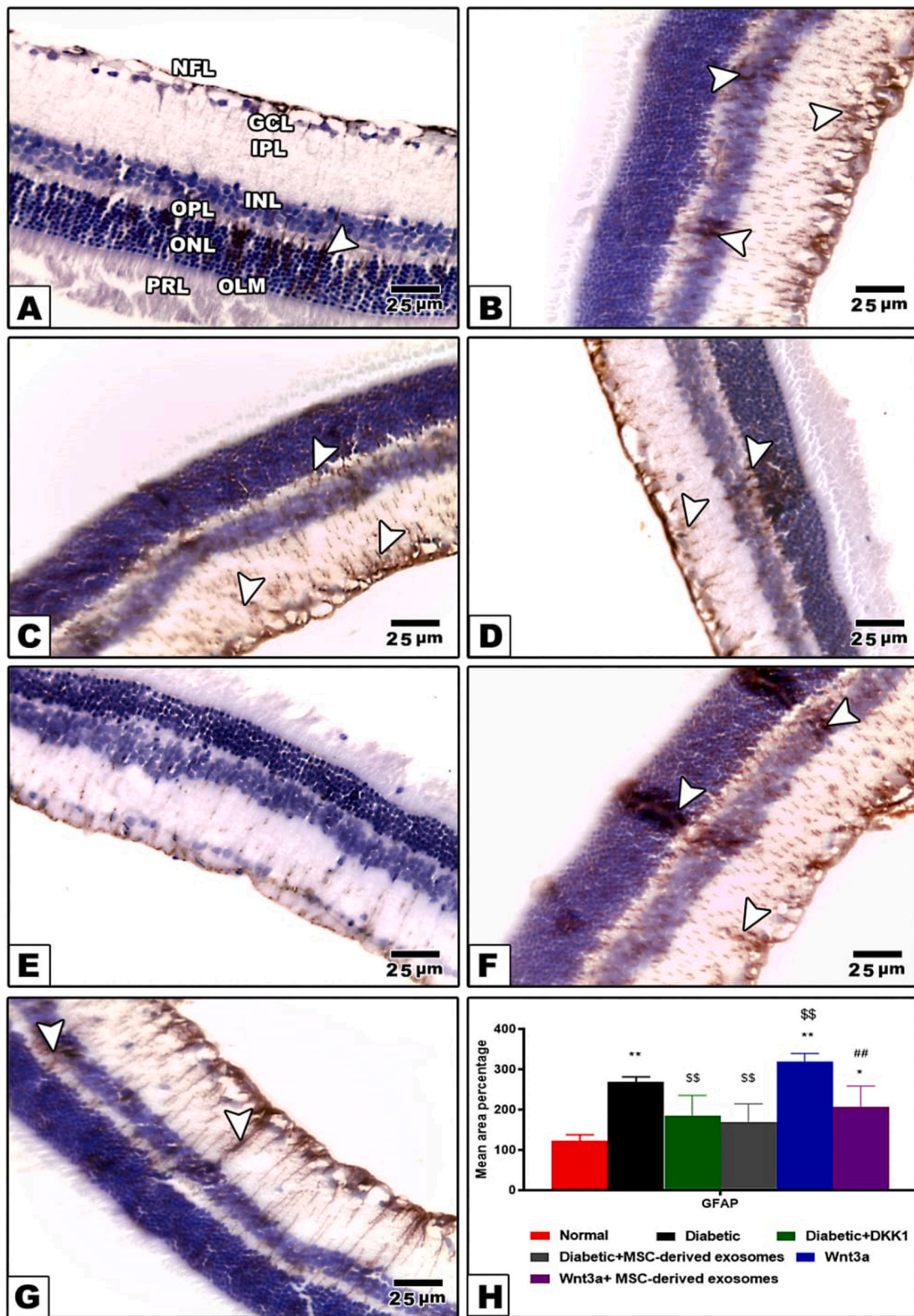


Fig. 10. GFAP immuno-stained sections from retinal tissues. (A) Control groups (group I) showed weak immunoreactivity for GFAP very close to GCL. (B, C, and F): Groups IIa, IIb, and V revealed strongly positive GFAP immunoreactivity in NFL and GCL, which was more prominent around blood capillaries in the innermost layers of retina and in Muller cell processes. (D and E): Groups III and IV showed minimal GFAP immunoreactivity within the Muller cell end feet. (G): Group VI revealed mildly positive GFAP immunoreactivity of Muller cell bodies and their processes. (H): Histogram representing the mean area percentage of GFAP immuno-reaction in all experimental groups. * represents significance in comparison with control group at $p < 0.05$, ** represents significance in comparison with control group at $p < 0.01$, \$ represents significance in comparison with diabetic group at $p < 0.05$, \$\$ represents significance in comparison with diabetic group at $p < 0.01$, ## represents significance in comparison with wnt3a group at $p < 0.01$. Data are expressed as mean \pm SE, (n = 6).

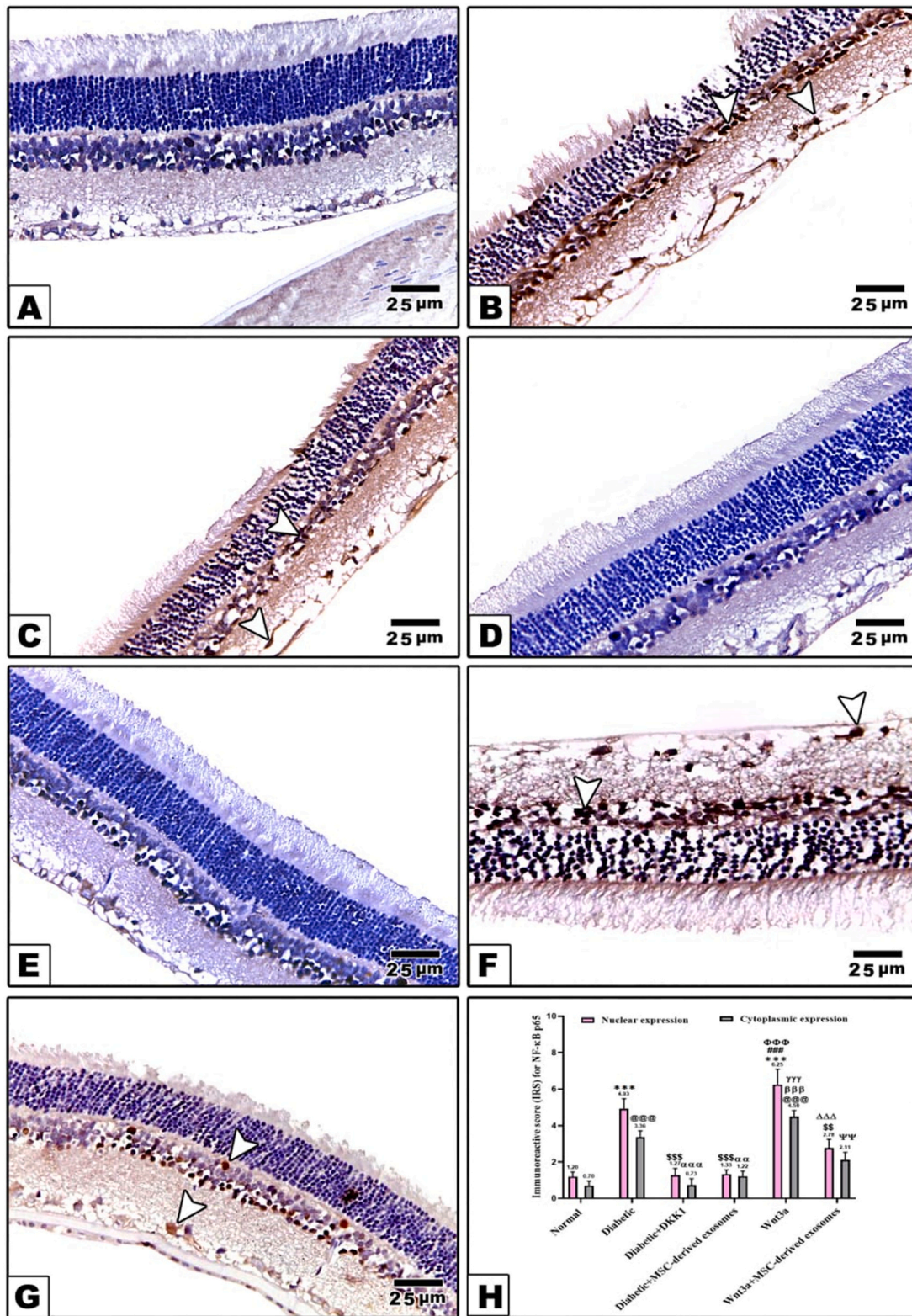


Fig. 11. NF-κB P65 immuno-stained sections from the retina. (A) Control groups (group I) showed no immunoreactivity for NF-κB P65. (B, C, and F): Groups IIa, IIb, and V revealed strongly positive NF-κB P65 immunoreactivity in GCL and INL. (D and E): Groups III and IV showed minimal NF-κB P65 immunoreactivity within GCL and INL. (G): Group VI revealed mildly positive NF-κB P65 immunoreactivity of GCL and INL. (H): Histogram representing immunoreactive score for NF-κB/p65 differentially in the nucleus and cytoplasm. Data are expressed as mean ± SE (n = 6). ***: p < 0.001 versus normal, \$\$\$: p < 0.001 versus diabetic group, @@@: p < 0.001 versus diabetic+DKK1 group, ΦΦΦ: p < 0.001 versus diabetic+ MSC-derived exosomes group and ΔΔΔ: p < 0.001 versus wnt3a group for nuclear expression, @@@: p < 0.001 versus normal, αα: p < 0.01, ααα: p < 0.001 versus diabetic group, βββ: p < 0.001 versus diabetic+DKK1 group, γγγ: p < 0.001 versus diabetic+ MSC-derived exosomes group and ΨΨΨ: p < 0.001 versus wnt3a group for cytoplasmic expression.

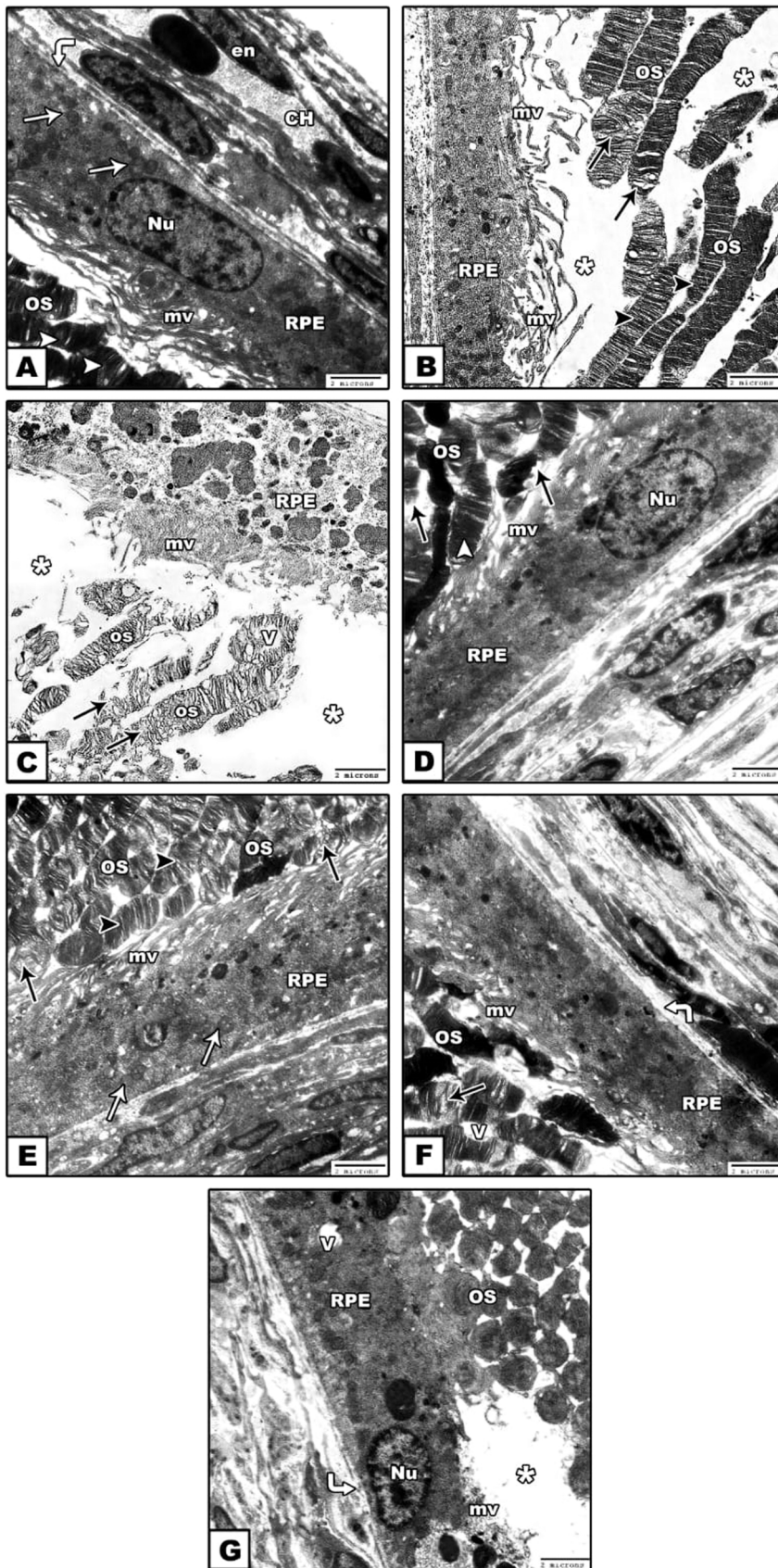


Fig. 12. Representative electron micrographs of retinal pigmented epithelial changes after exosomes administration. (A): Group I (control) showed an area of retinal pigment epithelial (RPE) with euchromatic oval nucleus (Nu), mitochondria (white arrow), and long apical microvilli (mv) surrounding elongated outer segments of the photoreceptor (OS) that showed parallel lamellar discs (arrow head). Note; The Choriocapillary layer (CH) appeared. (B): Group IIa showed short broken apical microvilli (mv) of RPE. Some outer segments (OS) are highly disorganized with distorted discs (black arrow) while, other discs appear normal (arrow head). Some areas showed lost OS (star). (C): Group IIb RPE short broken or absent apical microvilli (mv). The outer segments (OS) were highly disorganized with distorted discs (black arrow) and vacuolation (v). wide areas showed lost OS (star). (D) Group III showed RPE with heterochromatic nucleus (Nu) and apical microvilli (mv). OS had some normal lamellar discs (arrow head) and some other had distorted discs (black arrow). (E): Group IV RPE had basal mitochondria (white arrow) and long microvilli (mv). The outer segments (OS) showed mostly nearly normal lamellar discs (arrow head) and few with slightly distorted discs (black arrow). (F) Group V RPE showed long microvilli (mv). Some discs of the OS were still disorganized (black arrow) and vacuolated (v). (G): Group IV RPE showed euchromatic nucleus (Nu), vacuolated cytoplasm (v), and highly distorted apical microvilli (mv). There was large area of lost OS (star). (TEM, X2000).

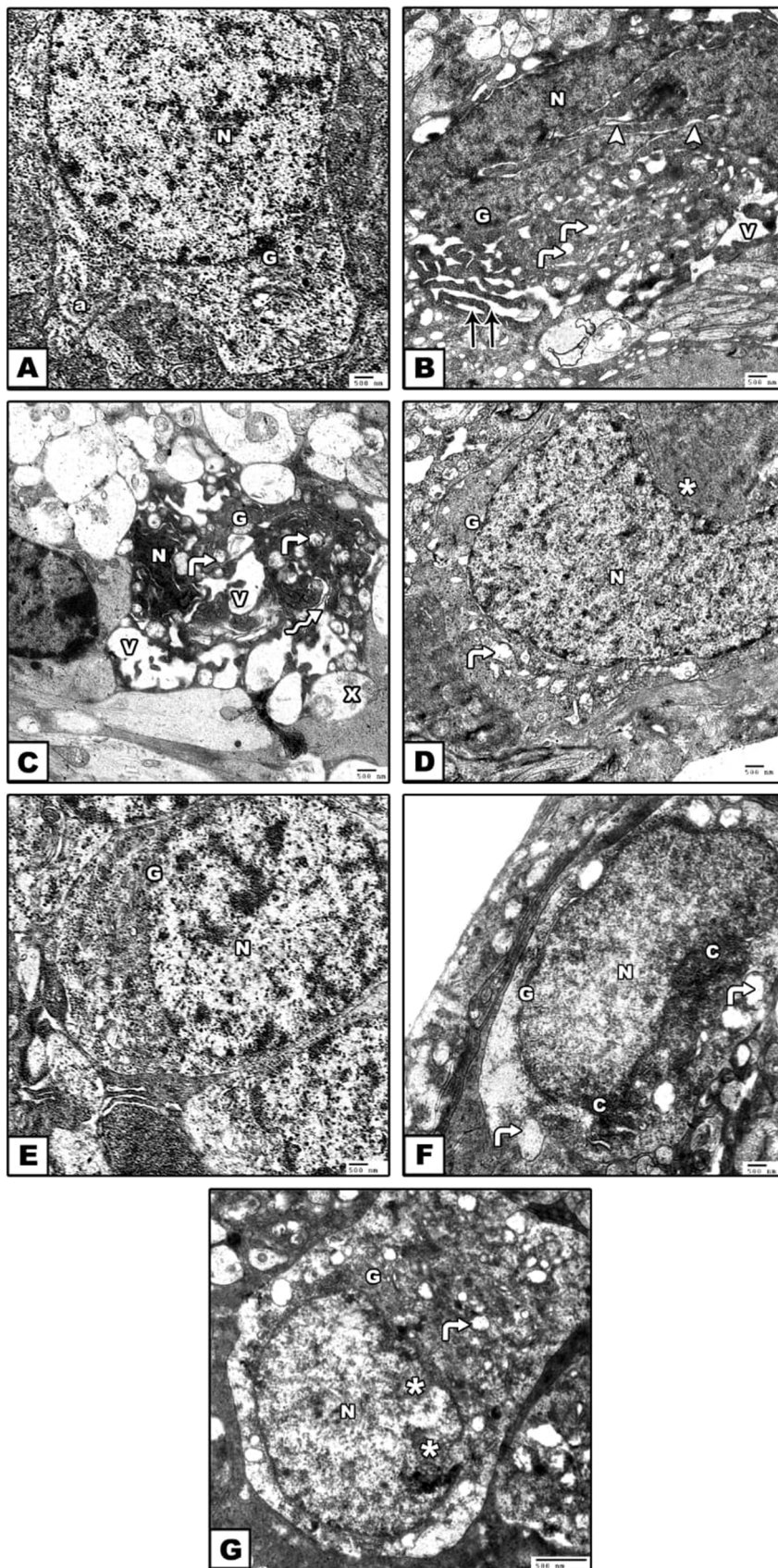


Fig. 13. Representative electron micrograph of Ganglion cell layers after exosomes administration. (A): Group I (control group) showed normal ganglion cells (G) had large euchromatic nucleus (N) and axon hillock (a). (B): Group IIa showed a degenerated ganglion cell (G). The cytoplasm displayed large irregular heterochromatic nucleus (N) with dilated nuclear envelope (arrow heads), dilated rER (double black arrows), vacuolations (v), and cristiolysis of mitochondria (angled arrow). (C): Group IIb showed a highly degenerated ganglion cell (G) with pyknotic nucleus (N). The cytoplasm showed vacuolations (v), cristiolysis of mitochondria (angled arrow), and irregular Golgi apparatus (wavy arrow). (D): Group III showed ganglion cell (G) displaying large euchromatic nucleus (N) with slight indentation (star). Note; Swollen mitochondria (angled arrow) with disintegrated cristae. (E): Group IV showed nearly normal ganglion cell (G) had large euchromatic nucleus (N). (F): Group V showed degenerated ganglion cell (G) displaying irregular nucleus (N) with areas of heterochromatin (c). Swollen mitochondria (angled arrow) with disintegrated cristae were present. (G): Group VI showed mildly degenerated ganglion cell (G) with large nucleus. Some mitochondria showed partial cristiolysis (angled arrow) while others, cytoplasm, SER and Golgi were broadly normal. (TEM, X3000).

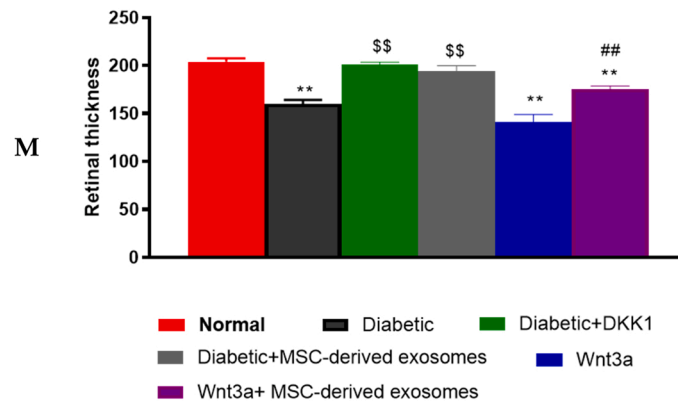
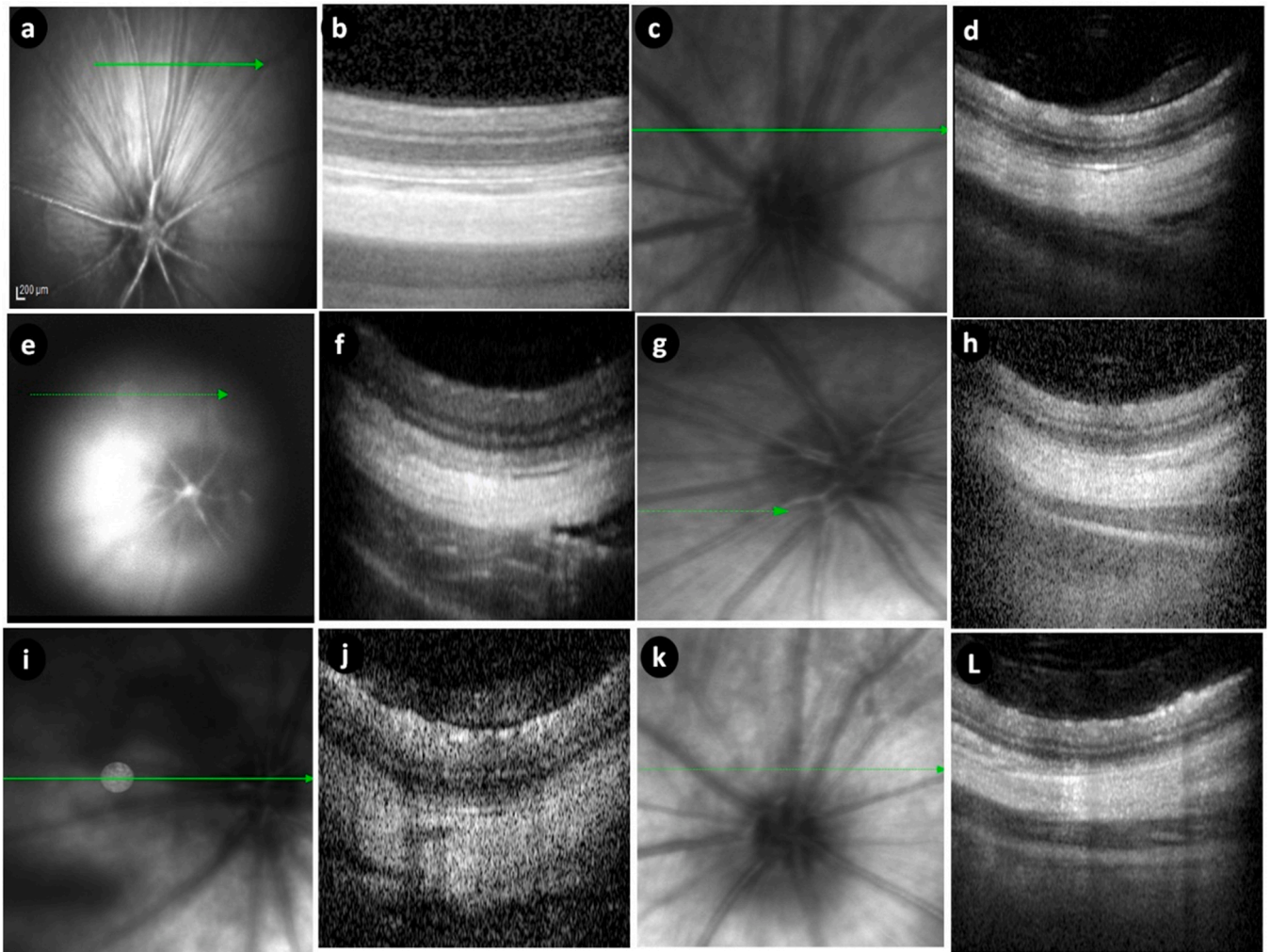


Fig. 14. Figure a-b: Fundus photo of a normal (Group I) retinal rat shows: normal retinal appearance, optic nerve head and vasculature. OCT scan of the retinal layers shows: normal appearance and thickness of all the retinal layers. Figure c-d: Fundus photo of a diabetic (Group II) retinal rat shows obscuration of the retinal appearance due to vitreous hemorrhage and venous beading (irregular dilatation of veins). OCT scan of the retinal layers shows: irregular appearance and reduction of all the retinal layers thickness due to neurological degeneration. Figure e-f: Fundus photo of retina from DKK1 treated rat (Group III) shows within normal retinal appearance, optic nerve head and vasculature. OCT scan of the retinal layers shows: within normal appearance and reduction of the inner retinal layers thickness. Figure g-h: Fundus photo of retinal rat from exosomes treated group (group IV) shows normal retinal appearance, optic nerve head and vasculature. OCT scan of the retinal layers shows: within normal appearance and thickness of all the retinal layers. Figure i-j: Fundus photo of Group V (Wnt3a group) retinal rat shows obscuration of the retinal appearance due to vitreous hemorrhage and attenuation of the retinal vasculature. OCT scan of the retinal layers shows: irregular appearance and reduction of all the retinal layers thickness due to neurological degeneration. Figure k-l: Fundus photo of Wnt3a and exosomes (group VI) retinal rat shows obscuration of the retinal appearance due to vitreous hemorrhage and attenuation of the retinal vasculature. OCT scan of the retinal layers shows: irregular appearance and reduction of all the retinal layers thickness due to neurological degeneration. Figure M: retinal thickness (micron).

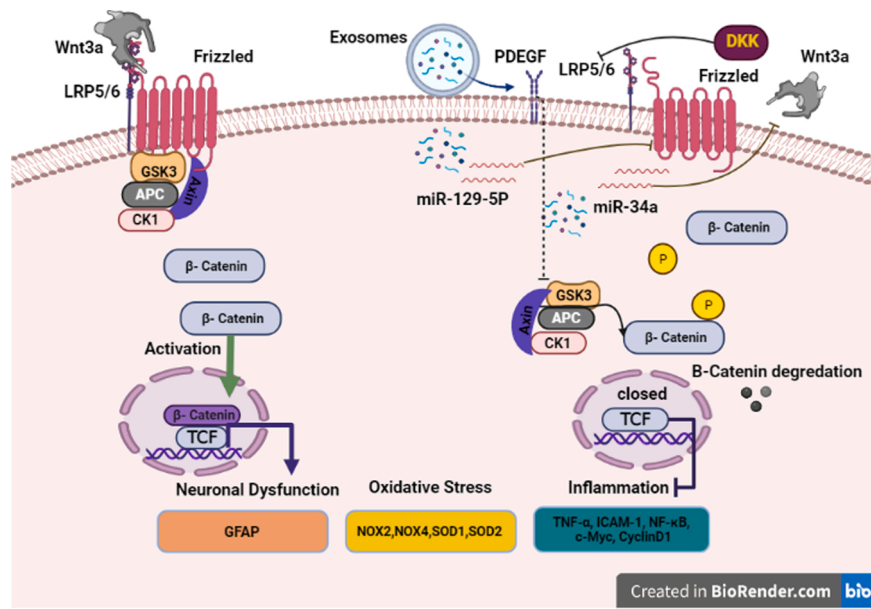


Fig. 15. Summary for proposed mechanisms of MSC-exosomes beneficial effects in diabetic retina.

[75] including *c-Myc*, *TNF- α* , *ICAM-1*, and *VEGF* [41], and other transcriptional regulators including nuclear factor κ B and signal transducer and activator of transcription 3 (STAT3) [76,77].

To confirm the Wnt signaling pathway activation in diabetic retina, DKK1 was intravitreally injected into diabetic rat eyes. In the DR models, an intravitreal injection of DKK1, a specific peptide inhibitor of the Wnt pathway is sufficient to mitigate retinal inflammation via blocking overexpression of pro-inflammatory factors such as ICAM-1 and COX-2. Correspondingly, DKK1 also decreased the retinal vascular leakage and enhanced the ischemia-induced retinopathy [7]. Furthermore, Wnt signaling blocking by DKK1 suppressed the ROS production induced by TNF- α and hyperglycemia. Recently, DKK1 was reported to inhibit the proliferation and migration of retinal pigment epithelial (RPE) cells. Further, expression of b-catenin and cyclin D1 were reduced in DKK1 over-expressing RPE cells [78]. Concomitant with these results, group III (DR+ DKK1 group) revealed inhibition of Wnt/b-catenin pathway with significant downregulation of LRP6, pLRP6, and total b-catenin with upregulation of P-b-catenin. These results were associated with significant downregulation of *Nox2*, *Nox4*, *Nox1* and upregulation of *SOD1*, *SOD2* mRNA and SOD activity. Further, significant downregulation of *VEGF*, *VE Cadherin*, *c-Myc*, *Cyclin-D1*, *ICAM-1*, and *TNF- α* indicated decreased retinal inflammation and ischemia highlighting that Wnt signaling played a key role in driving upregulation of these angiogenic and inflammatory factors. Histopathological observations reinforced these conclusions where retinal tissues showed increased retinal thickness, small, congested blood vessels. and significant reduction in iNOS, VEGF, NF κ B and GFAP expression when compared to group II.

Stem cells are widely studied for their potential therapeutic role in microvascular disorders. Recent observations indicate that cellular release of paracrine factors mediates an element of therapeutic efficacy of stem cells in affected tissues [79]. Indeed, cells through their exosomes are capable of secretion of various molecules/factors, including growth factors, nucleic acid, proteasomes, proteins, and antioxidants [80]. Stem cell-derived exosomes are also described as having roles in retinal protection via reduction of oxidative stress, inhibition of endothelial dysfunction, as well as limiting inflammatory responses [81,82]. Therefore, MSC-derived exosomes may provide therapeutic potential for patients suffering from DR. Interestingly, a recent comparative analysis of exosomes isolated from bone marrow, adipose tissue and umbilical cord stem cells suggested superiority of exosomes separated from bone

marrow derived MSCs in context of regeneration ability[83].

The therapeutic potential of bone marrow MSCs-derived exosomes in DR can potentially be attributed to the presence of exosomal microRNAs (miRs). MSC derived exosomes have revealed the presence of multiple miRNAs regulating Wnt/b-catenin pathways such as miR-129e5p [84] and miR-34a [85]. Recently, Wang et al. [38] established the critical roles of miR-129-5p in diabetes via targeting FZD4 to inhibit the b-catenin signaling pathway. *FZD4* is a member of the frizzled gene family, coupled with Wnt/b-catenin signaling pathway, and is vital in DR. miR-129e5p is predicted to target the 30 UTR of FZD4 [86] and its overexpression repressed FZD4 30 UTR reporter gene luciferase activity. Further, deletion of the 7 nt continuous matching sites complementary to miR-129e5p in the 30 UTR of FZD4 (FZD4-30 UTR-Mut) reduced this inhibition, confirming specificity of this effect, while a MiR-129e5p mimic significantly downregulated FZD4 protein compared with the control group [87]. Moreover, Zhu et al. [39] revealed that miR-34a down-regulated the expression of Wnt/b-catenin signaling pathway by targeting β -catenin gene. Anti-miR-34a significantly relieved b-catenin repression, its downstream genes, *c-myc* and *Cyclin D1*, and the S-phase cell cycle arrest. MSC-derived exosomes also possess surface receptors such as PDGFRB, which inhibit GSK3 β signaling, via its induction of the PI3K/Akt pathway, and interrupts the b-catenin signaling pathway [88, 89]. The observations derived from the MSC-derived exosomes treated group (group IV) were similar to those of group III (DKK1 group), indicating that MSC-derived exosomes potentially exerted their action through Wnt/b-catenin inhibition.

To confirm the blocking effect of the MSC-derived exosomes on Wnt pathway activation, we supplemented the animals with wnt3a, a ligand of Wnt pathway, followed by treatment with MSC-derived exosomes (group VI). Analysis of Wnt pathway components revealed up-regulated total b-catenin by Wnt3a in group V of the current study. However, this effect was inhibited by concomitant administration of MSC-derived exosomes in group VI. Meanwhile, the level of p-b-catenin, an indicator of the degradation of b-catenin and inactivation of Wnt pathway, showed the opposite trend to total b-catenin. Furthermore, Wnt3a in group V induced upregulation of *VEGF*, *VE Cadherin*, *c-Myc*, *Cyclin-D1*, *ICAM-1*, *TNF- α* , *Nox1*, *Nox2*, *Nox4* transcripts and this upregulation was blocked by co-treatment with MSC-derived exosomes in group VI. Likewise, MSC-derived exosomes reduced iNOS, VEGF, NF κ B and GFAP protein levels induced by Wnt3a. Further, Wnt target gene expression displayed non-significant changes between the DKK1 treated group and

the group treated with both Wnt3a and MSC-derived exosomes. These results indicated that both MSC-derived exosomes and DKK1 blocked Wnt pathway activation.

5. Conclusion

In the present study, we have demonstrated that MSC-exosomes suppress the Wnt/ b-catenin pathway in diabetes-induced retinal injury with subsequent reduction of oxidative stress, inflammation and angiogenesis, Fig. 15.

Funding

The work was supported by AlMaarefa Researchers Supporting program (MA-006), AlMaarefa University, Riyadh, Saudi Arabia.

CRedit authorship contribution statement

Conceptualization, NS, OB, NME and RS; Data curation, NS, OB, AH, HAA, NA, HTE, NS, OM, NME and RS; Formal analysis, OB, AH, HAA, HTE, HSE, OM, DS, NME and RS; Funding acquisition, NS and RS; Investigation, NS, OH, NE, OB, AH, HAA, NA, HTE, HSE, MA, ME, OM, NME and HA; Methodology, NS, OB, HAA, DS and MF; Resources, NS, OB, AH, NA, MA, ME, NS, GS, DS, MF and HA; Software, NS, OB, AH, HTE, ME and MF; Supervision, OH and NF; Validation, NS, OH, NE, OB, AH, HAA, NA, HTE, HSE, MA, ME, NS, GS, OM, NME, RS and HA; Visualization, NS, OH, NE, OB, HAA, NA, HTE, HSE, MA, ME, NS, GS, OM, NME, RS and HA; Writing – original draft, NS, OB, NF, NME and RS; Writing – review & editing, NS, OB, NF, NME and RS.

Ethics approval and consent to participate

This study was carried out in strict accordance with the recommendations in the Guide for the Care and Use of Laboratory Animals of the National Institutes of Health (NIH publication No. 85–23, revised 1996). All protocols were approved by the institutional review board for animal experiments of the Faculty of Medicine, Benha University, Egypt.

Consent for publication

Not applicable.

Declaration of of conflicting interests

The authors declare that they have no known competing financial interests or personal relationships that could have appeared to influence the work reported in this paper.

Availability of data and materials

The data that support the findings of this study are available from the authors upon reasonable request from the corresponding author.

Acknowledgment

not applicable.

References

- [1] K. Zhang, L. Zhang, R.N. Weinreb, Ophthalmic drug discovery: novel targets and mechanisms for retinal diseases and glaucoma, *Nat. Rev. Drug Discov.* 11 (7) (2012) 541–559.
- [2] S. Alzahrani, S.M. Ajwah, S.Y. Alsharif, E. Said, M. El-Sherbiny, S.A. Zaitone, M. Al-Shabrawey, N.M. Elsherbiny, Isoliquiritigenin downregulates miR-195 and attenuates oxidative stress and inflammation in STZ-induced retinal injury, *Naunyn-Schmiede's Arch. Pharmacol.* 393 (12) (2020) 2375–2385.
- [3] N.H. Cho, J.E. Shaw, S. Karuranga, Y. Huang, J.D. da Rocha Fernandes, A. W. Ohlrogge, et al., IDF Diabetes Atlas: global estimates of diabetes prevalence for 2017 and projections for 2045, *Diabetes Res. Clin. Pract.* (2018) 8:271–81.
- [4] T.M. Curtis, T.A. Gardiner, A.W. Stitt, Microvascular lesions of diabetic retinopathy: clues towards understanding pathogenesis? *Eye* 23 (7) (2009) 1496–1508.
- [5] E. Rechtman, A. Harris, H.J. Garzozzi, T.A. Ciulla, Pharmacologic therapies for diabetic retinopathy and diabetic macular edema, *Clin. Ophthalmol.* 1 (4) (2007) 383–391.
- [6] P.M. Titchenell, D.A. Antonetti, Using the past to inform the future: anti-VEGF therapy as a road map to develop novel therapies for diabetic retinopathy, *Diabetes* 62 (6) (2013) 1808–1815.
- [7] Q. Chen, J.-X. Ma, Canonical Wnt signaling in diabetic retinopathy, *Vis. Res.* 139 (2017) 47–58.
- [8] K. Park, K. Lee, B. Zhang, T. Zhou, X. He, G. Gao, et al., Identification of a novel inhibitor of the canonical Wnt pathway, *Mol. Cell Biol.* 31 (14) (2011) 3038–3051.
- [9] E. Dejana, The role of wnt signaling in physiological and pathological angiogenesis, *Circ. Res.* 107 (8) (2010) 943–952.
- [10] M. Sen, G. Ghosh, Transcriptional outcome of Wnt-Frizzled signal transduction in inflammation: evolving concepts, *J. Immunol.* 181 (7) (2008) 4441–4445.
- [11] H. Ouyang, Y. Zhuo, K. Zhang, WNT signaling in stem cell differentiation and tumor formation, *J. Clin. Investig.* 123 (4) (2013) 1422–1424.
- [12] H.-J. Choi, H. Park, H.-W. Lee, Y.-G. Kwon, The Wnt pathway and the roles for its antagonists, DKKs, in angiogenesis, *IUBMB Life* 64 (9) (2012) 724–731.
- [13] C. Toomes, H.M. Bottomley, R.M. Jackson, K.V. Towns, S. Scott, D.A. Mackey, et al., Mutations in LRP5 or FZD4 underlie the common familial exudative vitreoretinopathy locus on chromosome 11q, *Am. J. Hum. Genet.* 74 (4) (2004) 721–730.
- [14] Q. Xu, Y. Wang, A. Dabdoub, P.M. Smallwood, J. Williams, C. Woods, et al., Vascular development in the retina and inner ear: control by Norrin and Frizzled-4, a high-affinity ligand-receptor pair, *Cell* 116 (6) (2004) 883–895.
- [15] Y. Chen, Y. Hu, T. Zhou, K.K. Zhou, R. Mott, M. Wu, et al., Activation of the Wnt pathway plays a pathogenic role in diabetic retinopathy in humans and animal models, *Am. J. Pathol.* 175 (6) (2009) 2676–2685.
- [16] X. Xing, S. Han, G. Cheng, Y. Ni, Z. Li, Z. Li, Proteomic analysis of exosomes from adipose-derived mesenchymal stem cells: a novel therapeutic strategy for tissue injury, *Biomed. Res. Int.* 2020 (2020), 6094562.
- [17] X. Xiong, Y. Sun, X. Wang, HIF1A/miR-20a-5p/TGFβ1 axis modulates adipose-derived stem cells in a paracrine manner to affect the angiogenesis of human dermal microvascular endothelial cells, *J. Cell Physiol.* 235 (3) (2020) 2091–2101.
- [18] S. Yin, C. Ji, P. Wu, C. Jin, H. Qian, Human umbilical cord mesenchymal stem cells and exosomes: bioactive ways of tissue injury repair, *Am. J. Transl. Res.* 11 (3) (2019) 1230–1240.
- [19] Y. Fang, Y. Zhang, J. Zhou, K. Cao, Adipose-derived mesenchymal stem cell exosomes: a novel pathway for tissues repair, *Cell Tissue Bank* 20 (2) (2019) 153–161.
- [20] Z. Wan, X. Gao, Y. Dong, Y. Zhao, X. Chen, G. Yang, et al., Exosome-mediated cell-cell communication in tumor progression, *Am. J. Cancer Res.* 8 (9) (2018) 1661–1673.
- [21] X.-X. Yang, C. Sun, L. Wang, X.-L. Guo, New insight into isolation, identification techniques and medical applications of exosomes, *J. Control Release* 308 (2019) 119–129.
- [22] D.K. Jeppesen, A.M. Fenix, J.L. Franklin, J.N. Higginbotham, Q. Zhang, L. J. Zimmerman, et al., Reassessment of Exosome Composition, *Cell* 177 (2) (2019) 428–445, e18.
- [23] H. Henriques-Antunes, R.M.S. Cardoso, A. Zonari, J. Correia, E.C. Leal, A. Jiménez-Balsa, et al., The Kinetics of Small Extracellular Vesicle Delivery Impacts Skin Tissue Regeneration, *ACS Nano* 13 (8) (2019) 8694–8707.
- [24] N. Feng, Y. Jia, X. Huang, Exosomes from adipose-derived stem cells alleviate neural injury caused by microglia activation via suppressing NF-κB and MAPK pathway, *J. Neuroimmunol.* 334 (2019) 15, 576996.
- [25] bayoumi heba, helal omyma, elazab nahla, salem nesrien. The potential therapeutic Effect of Mesenchymal stem cells and their exosomes on experimentally induced diabetic retinopathy in rats: Histological and immunohistochemical study. *Egyptian Journal of Histology.* 2019 Nov 3;0(0):0–0.
- [26] C. Gu, H. Zhang, Y. Gao, Adipose mesenchymal stem cells-secreted extracellular vesicles containing microRNA-192 delays diabetic retinopathy by targeting ITGA1, *J. Cell Physiol.* 236 (7) (2021) 5036–5051.
- [27] J.E. Baulch, M.M. Acharya, B.D. Allen, N. Ru, N.N. Chmielewski, V. Martirosian, et al., Cranial grafting of stem cell-derived microvesicles improves cognition and reduces neuropathology in the irradiated brain, *Proc. Natl. Acad. Sci. USA* 113 (17) (2016) 4836–4841.
- [28] H. Xu, G. Zhao, Y. Zhang, H. Jiang, W. Wang, D. Zhao, et al., Mesenchymal stem cell-derived exosomal microRNA-133b suppresses glioma progression via Wnt/β-catenin signaling pathway by targeting EZH2, *Stem Cell Res Ther.* 10 (1) (2019) 381.
- [29] S. Bruno, C. Grange, F. Collino, M.C. Deregibus, V. Cantaluppi, L. Biancone, et al., Microvesicles derived from mesenchymal stem cells enhance survival in a lethal model of acute kidney injury, *PLoS One* 7 (3) (2012), e33115.
- [30] N. Ebrahim, I.A. Ahmed, N.I. Hussien, A.A. Dessouky, A.S. Farid, A.M. Elshazly, et al., Mesenchymal Stem Cell-Derived Exosomes Ameliorated Diabetic Nephropathy by Autophagy Induction through the mTOR Signaling Pathway, *Cells* 7 (12) (2018), E226.
- [31] S. Gatti, S. Bruno, M.C. Deregibus, A. Sordi, V. Cantaluppi, C. Tetta, et al., Microvesicles derived from human adult mesenchymal stem cells protect against

- ischaemia-reperfusion-induced acute and chronic kidney injury, *Nephrol. Dial. Transpl.* 26 (5) (2011) 1474–1483.
- [32] A. Lange-Consiglio, C. Perrini, G. Albini, S. Modina, V. Lodde, E. Orsini, et al., Oviductal microvesicles and their effect on *in vitro* maturation of canine oocytes, *Reproduction* 154 (2) (2017) 167–180.
- [33] J. Riegler, A. Liew, S.O. Hynes, D. Ortega, T. O'Brien, R.M. Day, et al., Superparamagnetic iron oxide nanoparticle targeting of MSCs in vascular injury, *Biomaterials* 34 (8) (2013) 1987–1994.
- [34] U. Altanerova, M. Babincova, P. Babinec, K. Benejova, J. Jakubecova, V. Altanerova, et al., Human mesenchymal stem cell-derived iron oxide exosomes allow targeted ablation of tumor cells via magnetic hyperthermia, *Int J. Nanomed.* 12 (2017) 7923–7936.
- [35] Suvama K.S., Layton C., Bancroft J.D. *Bancroft's Theory and Practice of Histological Techniques E-Book*. [Internet]. Philadelphia: Elsevier; 2018 [cited 2021 Aug 18]. Available from: <https://public.ebookcentral.proquest.com/choice/publicfullrecord.aspx?p=5321317>.
- [36] A.K. Patel, K.K. Park, A.S. Hackam, Wnt signaling promotes axonal regeneration following optic nerve injury in the mouse, *Neuroscience* 343 (2017) 372–383.
- [37] N. Ebrahim, H.A. Al Saihati, A. Shaman, A.A. Dessouky, A.S. Farid, N.I. Hussien, et al., Bone marrow-derived mesenchymal stem cells combined with gonadotropin therapy restore postnatal oogenesis of chemo-ablated ovaries in rats via enhancing very small embryonic-like stem cells, *Stem Cell Res Ther.* 12 (1) (2021) 517.
- [38] J. Wang, Y. Xia, J. Li, W. Wang, miR-129-5p in exosomes inhibits diabetes-associated osteogenesis in the jaw via targeting FZD4, *Biochem Biophys. Res Commun.* 566 (2021) 87–93.
- [39] L. Zhu, J. Gao, K. Huang, Y. Luo, B. Zhang, W. Xu, miR-34a screened by miRNA profiling negatively regulates Wnt/ β -catenin signaling pathway in Aflatoxin B1 induced hepatotoxicity, *Sci. Rep.* 5 (2015) 16732.
- [40] Suvama K.S., Layton C., Bancroft J.D., editors. *Theory and practice of histological techniques*. 7. ed. Edinburgh: Elsevier Churchill Livingstone; 2013. 637 p.
- [41] K.K. Zhou, S. Benyajati, Y. Le, R. Cheng, W. Zhang, J. Ma, Interruption of Wnt signaling in Müller cells ameliorates ischemia-induced retinal neovascularization, *PLoS One* 9 (10) (2014), e108454.
- [42] D. Navaratna, P.G. McGuire, G. Menicucci, A. Das, Proteolytic degradation of VE-cadherin alters the blood-retinal barrier in diabetes, *Diabetes* 56 (9) (2007) 2380–2387.
- [43] R.N. Frank, Diabetic retinopathy, *N. Engl. J. Med.* 350 (1) (2004) 48–58.
- [44] Y. Shao, T.-T. Xu, C.-G. Zhang, C.-G. Pei, Q. Zhou, The use of optical coherence tomography (OCT) to evaluate the efficacy of different photo-coagulations in diabetic macular edema treatment, *Eur. Rev. Med Pharm. Sci.* 20 (14) (2016) 2993–2998.
- [45] D. Navaratna, G. Menicucci, J. Maestas, R. Srinivasan, P. McGuire, A. Das, A peptide inhibitor of the urokinase/urokinase receptor system inhibits alteration of the blood-retinal barrier in diabetes, *FASEB J.* 22 (9) (2008) 3310–3317.
- [46] R. Klein, Hyperglycemia and microvascular and macrovascular disease in diabetes, *Diabetes Care* 18 (2) (1995) 258–268.
- [47] T. Zhou, K.K. Zhou, K. Lee, G. Gao, T.J. Lyons, R. Kowluru, et al., The role of lipid peroxidation products and oxidative stress in activation of the canonical wingless-type MMTV integration site (WNT) pathway in a rat model of diabetic retinopathy, *Diabetologia* 54 (2) (2011) 459–468.
- [48] K. Lee, Y. Hu, L. Ding, Y. Chen, Y. Takahashi, R. Mott, et al., Therapeutic potential of a monoclonal antibody blocking the Wnt pathway in diabetic retinopathy, *Diabetes* 61 (11) (2012) 2948–2957.
- [49] Y. Chen, Y. Hu, G. Moiseyev, K.K. Zhou, D. Chen, J. Ma, Photoreceptor degeneration and retinal inflammation induced by very low-density lipoprotein receptor deficiency, *Micro Res* 78 (1) (2009) 119–127.
- [50] M. Lin, Y. Chen, J. Jin, Y. Hu, K.K. Zhou, M. Zhu, et al., Ischaemia-induced retinal neovascularisation and diabetic retinopathy in mice with conditional knockout of hypoxia-inducible factor-1 in retinal Müller cells, *Diabetologia* 54 (6) (2011) 1554–1566.
- [51] Y. Saxena, B. Purwar, H. Meena, P. Sarthi, *Dolichos biflorus* Linn. ameliorates diabetic complications in streptozotocin induced diabetic rats, *Ayu* 35 (4) (2014) 442–446.
- [52] Q.-H. Yang, Y. Zhang, J. Jiang, M.-M. Wu, Q. Han, Q.-Y. Bo, et al., Protective effects of a novel drug RC28-E blocking both VEGF and FGF2 on early diabetic rat retina, *Int J. Ophthalmol.* 11 (6) (2018) 935–944.
- [53] S.M. Craige, K. Chen, Y. Pei, C. Li, X. Huang, C. Chen, et al., NADPH oxidase 4 promotes endothelial angiogenesis through endothelial nitric oxide synthase activation, *Circulation* 124 (6) (2011) 731–740.
- [54] C. Kleinschnitz, H. Grund, K. Wiegler, M.E. Armitage, E. Jones, M. Mittal, et al., Post-stroke inhibition of induced NADPH oxidase type 4 prevents oxidative stress and neurodegeneration, *PLoS Biol.* 8 (9) (2010), e1000479.
- [55] J. Li, J.J. Wang, S.X. Zhang, NADPH oxidase 4-derived H₂O₂ promotes aberrant retinal neovascularization via activation of VEGF receptor 2 pathway in oxygen-induced retinopathy, *J. Diabetes Res* 2015 (2015), 963289.
- [56] J. Li, J.J. Wang, Q. Yu, K. Chen, K. Mahadev, S.X. Zhang, Inhibition of reactive oxygen species by Lovastatin downregulates vascular endothelial growth factor expression and ameliorates blood-retinal barrier breakdown in db/db mice: role of NADPH oxidase 4, *Diabetes* 59 (6) (2010) 1528–1538.
- [57] A. Taddei, C. Giampietro, A. Conti, F. Orsenigo, F. Breviaro, V. Pirazzoli, et al., Endothelial adherens junctions control tight junctions by VE-cadherin-mediated upregulation of claudin-5, *Nat. Cell Biol.* 10 (8) (2008) 923–934.
- [58] M. Al-Shabraway, S. Smith, Prediction of diabetic retinopathy: role of oxidative stress and relevance of apoptotic biomarkers, *EPMA J.* 1 (1) (2010) 56–72.
- [59] Y. Funato, T. Michiue, M. Asashima, H. Miki, The thioredoxin-related redox-regulating protein nucleoredoxin inhibits Wnt-beta-catenin signalling through dishevelled, *Nat. Cell Biol.* 8 (5) (2006) 501–508.
- [60] S. Kajla, A.S. Mondol, A. Nagasawa, Y. Zhang, M. Kato, K. Matsuno, et al., A crucial role for Nox 1 in redox-dependent regulation of Wnt- β -catenin signaling, *FASEB J.* 26 (5) (2012) 2049–2059.
- [61] Q. Liu, X. Zhang, R. Cheng, J.-X. Ma, J. Yi, J. Li, Salutary effect of fenofibrate on type 1 diabetic retinopathy via inhibiting oxidative stress-mediated Wnt/ β -catenin pathway activation, *Cell Tissue Res* 376 (2) (2019) 165–177.
- [62] D.-Y. Zhang, Y. Pan, C. Zhang, B.-X. Yan, S.-S. Yu, D.-L. Wu, et al., Wnt/ β -catenin signaling induces the aging of mesenchymal stem cells through promoting the ROS production, *Mol. Cell Biochem* 374 (1–2) (2013) 13–20.
- [63] X. Zhang, J.P. Gaspard, D.C. Chung, Regulation of vascular endothelial growth factor by the Wnt and K-ras pathways in colonic neoplasia, *Cancer Res* 61 (16) (2001) 6050–6054.
- [64] H. Noma, H. Funatsu, H. Yamashita, S. Kitano, H.K. Mishima, S. Hori, Regulation of angiogenesis in diabetic retinopathy: possible balance between vascular endothelial growth factor and endostatin, *Arch. Ophthalmol.* 120 (8) (2002) 1075–1080.
- [65] S. Liebner, M. Corada, T. Bangsow, J. Babbage, A. Taddei, C.J. Czupalla, et al., Wnt/beta-catenin signaling controls development of the blood-brain barrier, *J. Cell Biol.* 183 (3) (2008) 409–417.
- [66] J. Chen, A. Stahl, N.M. Krah, M.R. Seaward, R.J. Dennison, P. Sapiieha, et al., Wnt signaling mediates pathological vascular growth in proliferative retinopathy, *Circulation* 124 (17) (2011) 1871–1881.
- [67] X. Ye, Y. Wang, H. Cahill, M. Yu, T.C. Badea, P.M. Smallwood, et al., Norrin, frizzled-4, and Lrp5 signaling in endothelial cells controls a genetic program for retinal vascularization, *Cell* 139 (2) (2009) 285–298.
- [68] M. Corada, D. Nyqvist, F. Orsenigo, A. Caprini, C. Giampietro, M.M. Taketo, et al., The Wnt/beta-catenin pathway modulates vascular remodeling and specification by upregulating Dll4/Notch signaling, *Dev. Cell* 18 (6) (2010) 938–949.
- [69] H.-W. Liu, Y. Meng, Y.-B. Ren, P. Sun, MicroRNA-15b participates in diabetic retinopathy in rats through regulating IRS-1 via Wnt/ β -catenin pathway, *Eur. Rev. Med Pharm. Sci.* 22 (16) (2018) 5063–5070.
- [70] H. Al-Hussaini, N. Kilarkaje, Effects of diabetes on retinal pigment epithelial cell proliferation and mitogen-activated protein kinase signaling in dark Agouti rats, *Exp. Toxicol. Pathol.* 67 (2) (2015) 117–124.
- [71] X. Zhang, L. Wen, Y. Chen, Y. Zhu, Vascular endothelial growth factor up-regulates the expression of intracellular adhesion molecule-1 in retinal endothelial cells via reactive oxygen species, but not nitric oxide, *Chin. Med J. (Engl.)* 122 (3) (2009) 338–343.
- [72] S. Ishida, T. Usui, K. Yamashiro, Y. Kaji, E. Ahmed, K.G. Carrasquillo, et al., VEGF164 is proinflammatory in the diabetic retina, *Invest Ophthalmol. Vis. Sci.* 44 (5) (2003) 2155–2162.
- [73] H. Funatsu, H. Noma, T. Mimura, S. Eguchi, S. Hori, Association of vitreous inflammatory factors with diabetic macular edema, *Ophthalmology* 116 (1) (2009) 73–79.
- [74] G.A. Limb, J. Hickman-Casey, R.D. Hollifield, A.H. Chignell, Vascular adhesion molecules in vitreous from eyes with proliferative diabetic retinopathy, *Invest Ophthalmol. Vis. Sci.* 40 (10) (1999) 2453–2457.
- [75] S. Portal-Núñez, D. Lozano, L.F. de Castro, A.R. de Gortázar, X. Nogués, P. Esbrit, Alterations of the Wnt/beta-catenin pathway and its target genes for the N- and C-terminal domains of parathyroid hormone-related protein in bone from diabetic mice, *FEBS Lett.* 584 (14) (2010) 3095–3100.
- [76] S. Yan, C. Zhou, W. Zhang, G. Zhang, X. Zhao, S. Yang, et al., beta-Catenin/TCF pathway upregulates STAT3 expression in human esophageal squamous cell carcinoma, *Cancer Lett.* 271 (1) (2008) 85–97.
- [77] K. Yamashina, H. Yamamoto, K. Chayama, K. Nakajima, A. Kikuchi, Suppression of STAT3 activity by Duplin, which is a negative regulator of the Wnt signal, *J. Biochem* 139 (2) (2006) 305–314.
- [78] J. Zhou, J. Jiang, S. Wang, X. Xia, DKK1 inhibits proliferation and migration in human retinal pigment epithelial cells via the Wnt/ β -catenin signaling pathway, *Exp. Ther. Med* 12 (2) (2016) 859–863.
- [79] Y. Wang, B. Fu, X. Sun, D. Li, Q. Huang, W. Zhao, et al., Differentially expressed microRNAs in bone marrow mesenchymal stem cell-derived microvesicles in young and older rats and their effect on tumor growth factor- β 1-mediated epithelial-mesenchymal transition in HK2 cells, *Stem Cell Res Ther.* 6 (2015) 185.
- [80] W. Zhang, S. Chen, M.-L. Liu, Pathogenic roles of microvesicles in diabetic retinopathy, *Acta Pharm. Sin.* 39 (1) (2018) 1–11.
- [81] L. Xie, M. Mao, L. Zhou, B. Jiang, Spheroid Mesenchymal Stem Cells and Mesenchymal Stem Cell-Derived Microvesicles: Two Potential Therapeutic Strategies, *Stem Cells Dev.* 25 (3) (2016) 203–213.
- [82] E. Moisseiev, J.D. Anderson, S. Oltjen, M. Goswami, R.J. Zawadzki, J.A. Nolte, et al., Protective Effect of Intravitreal Administration of Exosomes Derived from Mesenchymal Stem Cells on Retinal Ischemia, *Curr. Eye Res* 42 (10) (2017) 1358–1367.
- [83] Z.-G. Wang, Z.-Y. He, S. Liang, Q. Yang, P. Cheng, A.-M. Chen, Comprehensive proteomic analysis of exosomes derived from human bone marrow, adipose tissue, and umbilical cord mesenchymal stem cells, *Stem Cell Res Ther.* 11 (1) (2020) 511.

- [84] T. Pant, M. Juric, Z.J. Bosnjak, A. Dhanasekaran, Recent Insight on the Non-coding RNAs in Mesenchymal Stem Cell-Derived Exosomes: Regulatory and Therapeutic Role in Regenerative Medicine and Tissue Engineering, *Front Cardiovasc Med* 8 (2021), 737512.
- [85] K. Asgarpour, Z. Shojaei, F. Amiri, J. Ai, M. Mahjoubin-Tehran, F. Ghasemi, et al., Exosomal microRNAs derived from mesenchymal stem cells: cell-to-cell messages, *Cell Commun. Signal* 18 (1) (2020) 149.
- [86] R.P.F. Abuna, F.S. Oliveira, H.B. Lopes, G.P. Freitas, R.R. Fernandes, A.L. Rosa, et al., The Wnt/ β -catenin signaling pathway is regulated by titanium with nanotopography to induce osteoblast differentiation, *Colloids Surf. B Biointerfaces* 184 (2019), 110513.
- [87] H.K. Choi, H. Yuan, F. Fang, X. Wei, L. Liu, Q. Li, et al., Tsc1 Regulates the Balance Between Osteoblast and Adipocyte Differentiation Through Autophagy/Notch1/ β -Catenin Cascade, *J. Bone Min. Res* 33 (11) (2018) 2021–2034.
- [88] A. Raghav, Z.A. Khan, V.K. Upadhyay, P. Tripathi, K.A. Gautam, B.K. Mishra, et al., Mesenchymal Stem Cell-Derived Exosomes Exhibit Promising Potential for Treating SARS-CoV-2-Infected Patients, *Cells* 10 (3) (2021) 587.
- [89] F. Peng, H. Yao, H.K. Akturk, S. Buch, Platelet-derived growth factor CC-mediated neuroprotection against HIV Tat involves TRPC-mediated inactivation of GSK 3beta, *PLoS One* 7 (10) (2012), e47572.